Interfacial Designs of MXenes for Mild Aqueous Zinc-Ion Storage

Guo, Rui; Chen, Chaofan; Bannenberg, Lars J.; Wang, Hao; Liu, Haozhe; Yu, Minghao; Sofer, Zdenek; Lei, Zhibin; Wang, Xuehang

DOI
10.1002/smtd.202201683

Publication date
2023

Document Version
Final published version

Published in
SMALL METHODS

small methods
www.small-methods.com

Interfacial Designs of MXenes for Mild Aqueous Zinc-Ion Storage

Rui Guo, Chaofan Chen, Lars J. Bannenberg, Hao Wang, Haozhe Liu, Minghao Yu, Zdenek Sofer, Zhibin Lei, and Xuehang Wang**

Limited Li resources, high cost, and safety risks of using organic electrolytes have stimulated a strong motivation to develop non-Li aqueous batteries. Aqueous Zn-ion storage (ZIS) devices offer low-cost and high-safety solutions. However, their practical applications are at the moment restricted by their short cycle life arising mainly from irreversible electrochemical side reactions and processes at the interfaces. This review sums up the capability of using 2D MXenes to increase the reversibility at the interface, assist the charge transfer process, and thereby improve the performance of ZIS. First, they discuss the ZIS mechanism and irreversibility of typical electrode materials in mild aqueous electrolytes. Then, applications of MXenes in different ZIS components are highlighted, including as electrodes for Zn^{2+} intercalation, protective layers of Zn anode, hosts for Zn deposition, substrates, and separators. Finally, perspectives are put forward on further optimizing MXenes to improve the ZIS performance.

1. Introduction

Excessive dependence on traditional fossil fuels has caused environmental problems and the energy crisis. The global "carbon neutrality" strategic goal forces society to pursue cleaner and more efficient new energy sources,[1–3] such as wind, solar, and tidal energy. Due to the intermittent characteristics of these renewable energy sources, large-scale energy storage devices are needed to store such energy.[4,5] Since Sony successfully developed lithium-ion batteries (LIBs) in 1991, LIBs have dominated the energy storage market in portable devices and electric vehicles.[6] However, limited lithium resources, high cost and safety risks of LIBs hamper their use for large-scale energy storage.[7–10] Recently, rechargeable aqueous Zn-ion batteries (ZIBs) have attracted significant attention as promising alternatives for large-scale stationary storage due to their inherent safety, environmental benignity, and high theoretical capacity of Zn.

In ZIBs, Mn/V-based oxides and Prussian blue analogs are typical candidates for the cathode, and Zn foil is often employed as the anode. The key challenge for current cathode materials lies in that a high capacity, high conductivity and long-term stability are difficult to realize simultaneously.[11–14] Meanwhile, Zn plating/stripping reactions occurring at the anode are accompanied by Zn dendrite growth and side reactions, resulting in a low Zn plat-

R. Guo, C. Chen, L. J. Bannenberg, H. Wang, H. Liu, X. Wang
Department of Radiation Science and Technology
Faculty of Applied Sciences
Delft University of Technology
Delft 2629JB, The Netherlands
E-mail: x.wang-22@tudelft.nl

R. Guo, Z. Lei
Key Laboratory of Applied Surface and Colloid Chemistry
MOE
Shaanxi Engineering Lab for Advanced Energy Technology
Shaanxi Key Laboratory for Advanced Energy Devices
School of Materials Science and Engineering
Shaanxi Normal University
Xi'an, Shaanxi 710119, China
E-mail: zblei@snnu.edu.cn

H. Wang
State Key Laboratory for Modification of Chemical Fibers and Polymer Materials
College of Materials Science and Engineering
Donghua University
Shanghai 201620, China

M. Yu
Faculty of Chemistry and Food Chemistry
Center for Advancing Electronics Dresden Technische Universität
Dresden Modulgebäude
01217 Dresden, Germany

Z. Sofer
Institute of Chemical Technology
University of Chemistry and Technology Prague
Prague 6 16628, Czech Republic

The ORCID identification number(s) for the author(s) of this article can be found under https://doi.org/10.1002/smtd.202201683

DOI: 10.1002/smtd.202201683

ing/stripping efficiency. All these issues make aqueous ZIBs suffer from a limited energy density and short cycle life. To improve the reversibility of Zn-ion storage (ZIS), hybrid Zn-ion capacitors (ZICs) have been developed by replacing either the anode or the cathode of a ZIB with a capacitor-type electrode.[15] For example, two representative ZICs use activated carbon (AC) as electrodes and have the configurations of AC (+)//Zn (−) (Type I)[15] and MnO_2 (+)//AC (−) (Type II),[16] with the latter one also being called "rocking-chair" configuration. Since such configurations blur the boundary between batteries and capacitors, we refer to both ZIBs and ZICs as ZIS devices in this paper to avoid any confusion. Although it has been shown that such strategies improve the reversibility, different energy storage mechanisms of the cathode and anode in ZICs lead to a mismatch in the capacity and kinetics.[17] Hence, there is an urgent need to develop electrode materials with excellent physical, chemical and electrochemical properties for high-performance ZIS in aqueous systems.

Interfacial design is crucial for the performance of ZIS devices as electrochemical reactions and charge transfer processes take place at the interface.[18–22] Highly conductive interfaces are beneficial to promote charge transfer processes.[23] The hydrophilic interface can facilitate the accessibility of solvated Zn^{2+} to the electrode materials.[24] The zincophilic interface is conducive to trapping Zn^{2+}, preventing 2D diffusion of Zn^{2+} on the surface of anode, inducing uniform nucleation and inhibiting dendrite growth.[25] The construction of 3D interface structures cannot only facilitate ion transport, but also increase the number of Zn^{2+} storage sites and alleviate the structural change of electrode material during charging and discharging.[26] In addition, the interface can act as a protective layer by preventing direct contact between the electrode and electrolyte, thereby inhibiting cathode dissolution,[27] anode corrosion, hydrogen evolution reaction (HER), and other side reactions.[28,29] The formation of the interface can be achieved by modifying the electrode, the separator or regulating the electrolyte with additives.[30,31] Furthermore, construction methods of the interface layer are usually divided into two categories: in-situ (physical or chemical vapor deposition, atomic or molecular layer deposition and chemical or electrochemical deposition) and ex-situ (doctor blading and spin-coating) methods depending on the type of electrode materials.[32,33] For example, coating the electrode with a polymer by doctor blading method can assist the desolvation of hydrated Zn^{2+} and limit the 2D diffusion of Zn^{2+} on the anode surface.[34] Modifying the separator with Zr-based MOF (UiO-66-GF) via a hydrothermal method accelerates the transport of charge carriers and provides a uniform electric field distribution on the surface of Zn anode, effectively inhibiting dendrites, improving corrosion resistance and suppressing the HER.[35] On the electrolyte side, the electrode-electrolyte interface can be optimized by adding different electrolyte additives to homogenize the local concentration of Zn^{2+},[36,37] accelerate the hydrated Zn^{2+} desolvation and migration,[38] or form solid electrolyte interphases to protect and stabilize the cathode[39] or anode.[40] However, most electrode interface materials are designed to realize a single function, such as improving the electronic conductivity, hydrophilicity or zincophilicity or homogenizing the electric field. Therefore, it is vital to develop interface materials with ease of preparation and integrated functions.

2D transition metal carbides and/or nitrides MXenes, commonly synthesized by selectively etching the A layer from MAX precursors, have a general formula $M_{n+1}X_nT_x$, where M represents one or multiple early transition metal(s) (Ti, V, Nb, Mo, etc.), X is C and/or N, and T_x represents surface functional groups such as O, OH, F and Cl.[41] These materials demonstrate competitive performances in various energy storage applications due to their unique physical and chemical properties.[42–48] The MXenes offer appealing interfaces for aqueous ZIS application for several reasons: i) The great electronic conductivity (~20000 S cm^{-1}) allows rapid electron transport in the MXene;[49] ii) High specific surface area of 2D MXene sheets are highly accessible for Zn^{2+} ions and the large interlayer space between MXene layers is beneficial for fast ion transport;[50] (iii) Rich and tunable surface groups make MXenes not only hydrophilic but also zincophilic. The hydrophilic nature is favorable for ion accessibility[51] while the zincophilicity of MXenes is beneficial for trapping Zn^{2+}, limiting the 2D diffusion of Zn^{2+} ions, inducing uniform deposition of Zn with a high lattice match between MXenes and Zn, thereby Zn^{2+} ions are guided to uniformly nucleate and grow in a planar manner on the (000l) crystal plane at the MXene interface;[52] iv) The flexibility and self-standing of MXenes make it possible to directly use MXene as a cathode electrode for storing Zn^{2+} ions, or as a substrate for Zn deposition (anode). Thus, a higher energy density could be obtained due to the lighter weight without any binder or additives. Furthermore, the interlayer spacing,[53] surface groups,[54] morphology[55] of MXene and heterostructures[56] can all be tuned to design MXene-based ZIS devices with improved performance. Although there have been several papers summarizing the application of MXenes for aqueous ZIS,[57–59] the interfacial design of MXenes-based cathodes and the application of MXene-based interfaces in anodes, separators, and substrates have not been summarized systematically. This review starts with discussing the mechanism and issues of typical ZIS electrodes in mild aqueous electrolytes to demonstrate the importance of interfaces (**Figure 1**). Then, we summarize the interfacial designs of MXenes that assist Zn^{2+} intercalations in the MXene-based cathodes and the applications of MXene-based interfaces (including protective layers, 3D networks, Zn-free anode, substrates, and separators) that increase the reversibility of Zn anodes. Finally, corresponding prospects are put forward based on the current research status.

2. Charge Storage Mechanism and Problems of Mild Aqueous Zinc-Ion Storage

A typical aqueous ZIS consists of a cathode (or a positive electrode), a Zn metal anode (or a negative electrode), and an aqueous electrolyte (mild acidic or neutral aqueous solution) (**Figure 2**a). The commonly used aqueous ZIS electrolytes usually contain one or more soluble zinc salts, such as $ZnSO_4$, $Zn(CH_3COO)_2$, $ZnCl_2$, $Zn(NO_3)_2$, zinc trifluoromethanesulfonate ($Zn(CF_3SO_3)_2$ or $Zn(OTF)_2$) and zinc bis(trifluoromethylsulfonyl)imide ($Zn(TFSI)_2$).[65,66] They have a mild acidic or neutral pH to eliminate the formation of passivating by-products (e.g., ZnO) typically formed in alkaline electrolytes.[67]

As illustrated in Figure 2a, there are many problems that need to be addressed for the practical application of ZIS devices,[35,69]

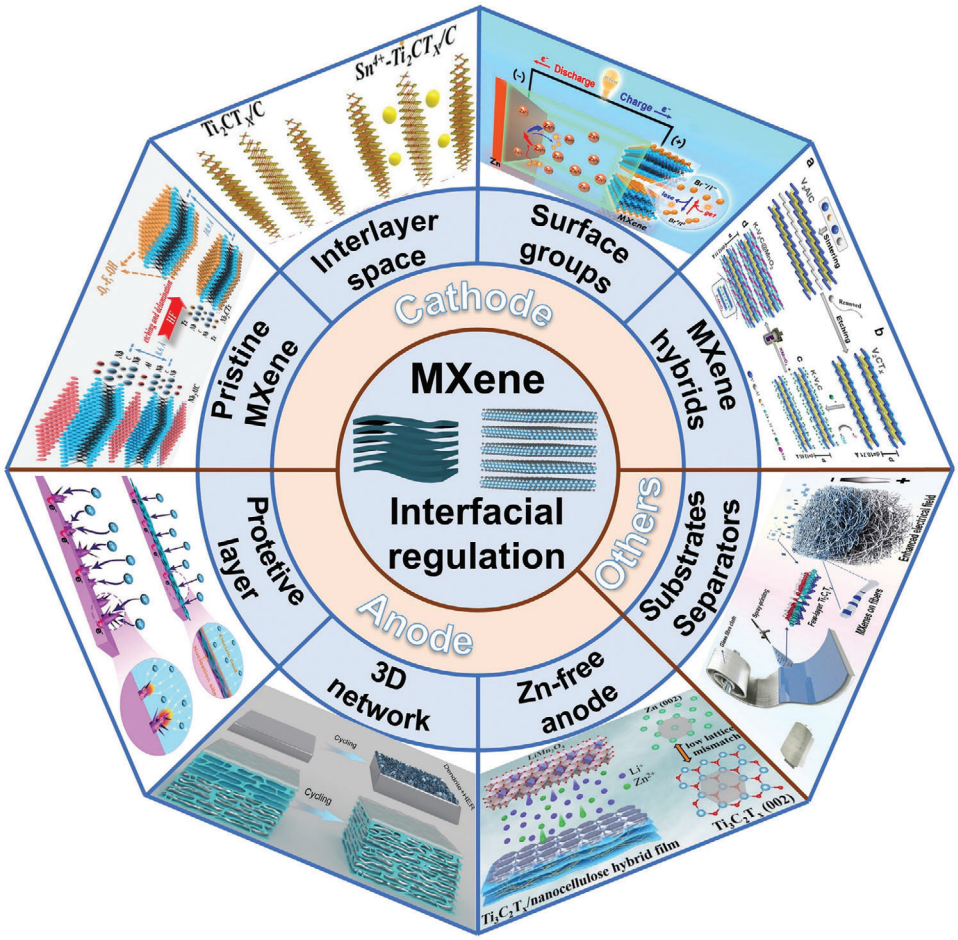

Figure 1. A summary of MXene interfacial regulation strategies towards anode, cathode, and other components for zinc-ion storage. Pristine MXene: Reproduced with permission.[60] Copyright 2021, Elsevier. Interlayer space: Reproduced with permission.[53] Copyright 2020, Wiley-VCH GmbH. Surface groups: Reproduced with permission.[54] Copyright 2021, American Chemical Society. MXene hybrids: Reproduced with permission.[61] Copyright 2021, American Chemical Society. Protective layer: Reproduced with permission.[28] Copyright 2020, Wiley-VCH GmbH. 3D network: Reproduced with permission.[62] Copyright 2021, Wiley-VCH GmbH. Zn-free anode: Reproduced with permission.[63] Copyright 2022, American Chemical Society. Substrates separators: Reproduced with permission.[64] Copyright 2022, Wiley-VCH GmbH.

including the dendrite formation, corrosion and hydrogen evolution reaction (HER) at the Zn anode surface,[70] as well as the dissolution, structural collapse and low electronic conductivity of the cathode.[12] These issues, mainly arising from irreversible electrochemical reactions/processes and slow kinetics, limit the overall performance of ZIS devices, including cycling life, rate capability, Coulombic efficiency, energy density and power density.

2.1. Charge Storage Mechanism and Problems of the Cathode

Charge storage in cathodes involves the insertion/extraction of Zn^{2+} in the host materials (including Mn-based oxides, V-based oxides, Prussian blue analogues, and poly-anion compounds).[71,72] Apart from being a low-cost, environmentally benign and abundant material, the ideal cathode material should feature a high capacity, high ionic and electronic conductivities and high structural stability to realize high (dis)charging rates and stable cycling performance.

2.1.1. Manganese oxides

Among the potential cathode materials, MnO_2 is traditionally used in Zn-ion primary batteries and is also the most widely explored cathode candidate in ZIBs due to its affordability and reasonable capacity (over 300 mAh g^{-1}).[73] However, the mechanisms involved are complex owing to different MnO_2 crystallographic polymorphs and nanostructures with strongly varying performance as the cathode.[74] In most cases, the intercalation of Zn^{2+} into the structure of MnO_2 is accompanied by the conversion of the pristine MnO_2 structure to spinel $ZnMn_2O_4$. Apart from a large volume change inducing the detachment of the active material from the current collector, the conversion reaction also results in the dissolution of Mn^{2+} in the aqueous electrolyte.[75]

In addition, co-insertion of protons with Zn^{2+} is frequently reported and significantly contributes to the overall capacity in mild acidic electrolytes, for instance, $ZnSO_4$.[76,77] The hydroxyl-termination of MnO_2 on the cathode surface facilitates proton

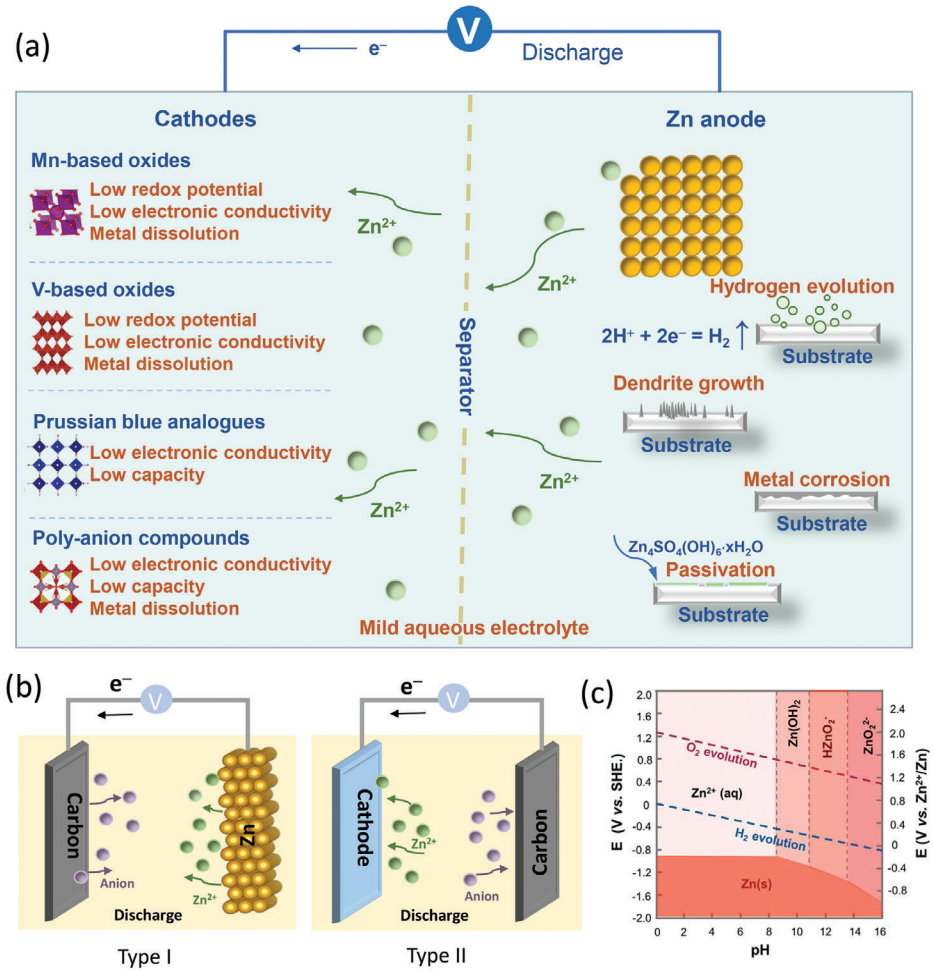

Figure 2. a) Schematic illustration of typical ZIB electrode materials and common issues in traditional aqueous ZIBs. b) Schematic illustration of typical ZICs. c) Pourbaix diagram of the Zn metal in aqueous solutions. Reproduced with permission.[68] Copyright 2020, American Chemical Society.

transfer across the electrode-electrolyte interface with a lower desolvation penalty compared to divalent Zn^{2+}, which enables reversible proton insertion.[77,78] Meanwhile, the resulting increase in pH caused by proton intercalation is buffered by the precipitation of $Zn_4(OH)_6SO_4{\cdot}xH_2O$ that is present at the electrode-electrolyte interface.[79] In sum, though reversible Zn^{2+} intercalation has been demonstrated in MnO_2, the abovementioned dissolution of Mn^{2+}, and the detachment of active material from the current collector caused by the large volume change during phase transformations result in a rapidly degrading cycling capacity and short lifespan.

2.1.2. Vanadium oxides

Compared to MnO_2, V-based oxides have been reported to endure Zn^{2+} intercalation without phase transformation, which results in promising capacity retention.[80] For example, ex-situ X-ray diffraction (XRD) and X-ray photoelectron spectroscopy have shown that Zn^{2+} can rapidly insert into the Li^+ pre-intercalated $V_2O_5{\cdot}nH_2O$ due to the enlarged interlayer spacing.[81] As a result, superior rate performance and great capacity retention of more than 80% over 1000 cycles can be obtained. Like MnO_2, the hydrophilic surface of vanadium oxides favors the insertion of protons. Thus, co-intercalation of protons and reversible precipitation of $Zn_4(OH)_6SO_4{\cdot}xH_2O$ have been proposed to dominate the electrochemical energy storage behavior of vanadium oxides. It is worth noting that the competition between H^+ and Zn^{2+} highly depends on the desolvation energy at the electrode-electrolyte interface. Due to the higher desolvation penalty of Zn^{2+}, only H^+ insertion reactions accompanied by reversible conversion and deposition process of $Zn_4(OH)_6SO_4{\cdot}5H_2O$ are reported for VO_2 cathodes.[82] The open tunnel structure and large interlayer spacing make V-based oxides promising candidates for ZIS with a high capacity (around 400 mAh g^{-1}), great rate capability, and long cycle life. However, a low redox potential at around 0.8 V compromises the energy density of V-based ZIBs.

2.1.3. Prussian blue analogues

Compared to V-based and Mn-based oxides, Prussian blue analogues enable ZIBs with higher output voltages (around 1.7 V). Besides, migration and intercalation of Zn^{2+} rather than H^+

dominate the charge storage process.[83] They exhibit superior rate performance owing to the intrinsic open framework structure, which allows for rapid Zn^{2+} intercalation. However, the low electronic conductivity, moderate capacity, and severe dissolution during cycling call for more efficient strategies to further improve their electrochemical performance.

2.1.4. Poly-anion compounds

There are only a few publications focusing on the charge storage mechanism of poly-anion compounds for ZIS and these publications focus mostly on phosphate materials.[84] The complexity of the electrochemical reaction lies in different insertion positions and migration pathways of Zn^{2+} in poly-anion structures. For instance, earlier studies show that Na^+ is first extracted from the 18e site of $Na_3V_2(PO_4)$ (NVP), and Zn^{2+} ions are subsequently inserted at both the 18e and 6b sites in NVP, a representative NASICON-structured poly-anion material.[83] Poly-anion compounds show superior structural stability and reasonable redox potential at around 1.4 V, but still suffer from low electronic conductivity, low specific capacity, and the dissolution of transition metal ions.

In general, the intrinsic moderate electronic conductivity of cathode materials and the interfacial desolvation of Zn^{2+} are the key issues that limit the rate performance of cathode material for ZIS. In addition, the dissolution of transition metal ions at the cathode-electrolyte interface leads to poor cycling stability and limits lifespan. Thus, reasonable interfacial design should be made to realize rapid electronic and ionic transport and address the dissolution problem to achieve further improvement in the performance of ZIS devices.

2.1.5. Carbon-based cathodes

When replacing the typical cathode material with a carbon-based material, the cycling stability of the cell improves as carbon-based materials store charges by forming the electric double layers.[85] Notably, the carbon electrodes should be referred to as positive electrodes as such cells are hybrid capacitors (or, namely ZICs). In this case, the anions in the electrolyte are reversible adsorbed/desorbed on the surface of the positive carbon electrode, while zinc deposition/stripping takes place on the Zn surface (Type I in Figure 2b).[86] However, the poor specific capacity of carbon materials and the mismatch kinetics with the Zn anode limits the energy density and rate performance of ZICs.[57,87] It is worth noting that there is another type of ZIC, or namely, "rocking-chair" ZICs (Type II in Figure 2b). Instead of replacing the cathode with a carbon-based electrode, the Zn anode is replaced by capacitor-type material while typical cathode materials still serve as the cathode in "rocking-chair" ZICs.[57,87] This configuration eliminates the corrosion and passivation of a Zn metal anode. However, in this case, the rate performance is limited by the cathode properties.

2.2. Chemical Reactions and Problems of the Zinc Anode

Zn metal is a promising anode owing to its large theoretical specific capacity (5855 mAh cm^{-3}, 820 mAh g^{-1}) and convenient redox potential ($Zn^{2+}/Zn = -0.763$ V versus SHE), i.e., low enough to provide a reasonable energy density and high enough to be compatible with aqueous electrolytes.[16,69,88] During the charge and discharge process, Zn^{2+} is reversibly plated on or stripped from the surface of Zn metal, or in an anode-free approach, on a (coated) current collector.[89,90] However, anode-related dendrite growth, the occurrence of the HER, and corrosion reactions[91] reduce the Coulombic efficiency and hence shorten the cycle life of the Zn anode.[70,92]

2.2.1. Zinc dendrite growth

The formation of Zn dendrites heavily depends on the changes in the electric field strength and electrolyte ion concentration.[93,94] Zn^{2+} ions, driven by the electric field, move to the anode surface through 2D diffusion and prefer to nucleate at sites where the electric field strength is higher to minimize the surface energy.[95] However, the nucleation sites with high electric field strength and gradients are often at edges or tips.[96] Accordingly, the uneven anode surface will accelerate the formation and growth of Zn dendrites. This continuous growth of Zn dendrites eventually produces "dead Zn", which easily pierces the separator and causes the short circuit resulting in poor cycle life and early death of ZIS devices.[97]

2.2.2. Corrosion reaction

Metal corrosion refers to the electrochemical and spontaneous chemical reactions between a metal and a surrounding medium, i.e., in this case, the Zn anode and the electrolyte. As the anode has a non-uniform surface, different potentials are present at different regions on the surface. As such, corrosion reactions enable the Zn electrode to form numerous corrosion micro-batteries in the aqueous solution. Zn metal loses electrons and fast dissolves in the electrolyte of these micro-batteries, corroding the Zn anode and forming hydroxides, which significantly reduces the cycling stability of the Zn anode.[70,98–100] Meanwhile, metal corrosion is usually accompanied by the HER, which is another major problem in the development of Zn anodes.

2.2.3. Hydrogen evolution reaction

Due to the slightly higher electronegativity of the hydrogen atom, Zn metal tends to react with water at the interface between the electrolyte and the anode.[101,102] Theoretically, the electrochemical potential of Zn^{2+}/Zn is much lower than that of H^+/H_2 across the entire pH region (Figure 2c).[68] This means that the corrosion reaction and the HER can take place spontaneously during charging and discharging or in the process of standing. In mild aqueous electrolytes, the HER can be expressed as:[68,92,94]

$$Zn + 2H_2O \rightarrow Zn^{2+} + OH^- + H_2 \uparrow \quad (1)$$

$$2H^+ + 2e^- \rightarrow H_2 \uparrow \quad (2)$$

However, the actual HER in aqueous battery systems is a more complex heterogeneous interfacial reaction. The occurrence of

the HER around Zn anodes requires a higher energy than the theoretical value. Therefore, the overpotential, an important electrochemical parameter to evaluate the gap between the theoretical and practical redox potentials, should be taken into consideration. The overpotential for the HER highly depends on the electrolyte pH, which makes Zn deposition possible without the HER on the Zn anode surface by adjusting the pH value of the electrolyte.[103] It is worth noting that the HER and corrosion reactions take place concurrently. The release of H_2 during charging will partially consume the electrons provided by the Zn anode, lowering the Coulombic efficiency of the Zn anode. The continuous H_2 evolution raises the gas pressure of the battery, which, in turn, accelerates the dendrite formation.

2.2.4. Passivation

In the mild electrolyte system, continuously released OH^- (generated during the HER) accumulates around the Zn anode. The OH^- reacts with Zn^{2+} and generates by-products covering the anode surface like $Zn(OH)_2$,[104,105] $Zn_4SO_4(OH)_6{\cdot}xH_2O$[106] and TFSI-based complexes.[67] As a result, a structurally loose and electrically insulating passivation layer is formed on the anode. This layer not only increases the ion diffusion resistance but also hinders rapid electron transport. The formation of a passivation layer leads to an increased surface heterogeneity of the Zn anode, further accelerating dendrite growth. These vicious reactions result in a low Coulombic efficiency and a short lifespan of the anode.[107,108]

In short, dendrite growth, corrosion, the HER, and the formation of a passivating layer are mutually interdependent. The uneven deposition of Zn during charging usually leads to the formation of dendrites which in turn accelerates the anode corrosion and HER. Meanwhile, due to the high electrochemical activity and thermodynamic instability, metallic Zn is vulnerable to oxidization in mild aqueous electrolytes. Hence, these issues need to be addressed simultaneously.[67,91,109,110]

3. MXenes in the Zn-Ion Storage Cathodes

3.1. Zn-Ion Intercalations in Pristine MXenes

Compared with traditional ZIS cathodes, the superior electronic conductivity and large interlayer space of MXenes ensure the rapid transportation of both electrons and Zn^{2+} ions. In addition, due to the unique 2D structure and strong M-X bond, Zn-ions are not inserted in the lattice of MXene, but intercalate between the flexible MXene interlayers, giving rise to minimal volume changes. The insertion of cations is usually accompanied by the interactions with surface groups of MXene, which subsequently lead to a minor change in the valence state of transition metals.[111] Thus, high-rate performance and cycling stability, which are the major limitations of traditional ZIS cathode materials, are not issues for MXene-based electrodes. So far, various MXenes have been directly applied as cathodes for ZIS, including $Ti_3C_2T_x$, Nb_2CT_x, V_2CT_x, and high-entropy MXenes (Table S1).

Early studies proposed that the charging process of a $Ti_3C_2T_x$ ZIS cathode involves the adsorption of SO_4^{2-} and desorption of Zn^{2+}, while the discharge process is dominated by the desorption of SO_4^{2-} and absorption of Zn^{2+}.[112] Recently, the reversible (de-)intercalation of Zn^{2+} in MXenes during (dis)charge has been demonstrated in a hexadecyltrimethylammonium bromide (CTAB)-pillared $Ti_3C_2T_x$.[113] No sulfur was detected by energy-dispersive X-ray spectroscopy in the discharged CTAB-pillared $Ti_3C_2T_x$, which implies that Zn^{2+} is the main charge carrier instead of SO_4^{2-}. Meanwhile, the Ti=O vibration peak in the Raman spectrum of Zn^{2+}-intercalated $Ti_3C_2T_x$ displays a shoulder at 210 cm^{-1}, suggesting the formation of Ti–O–Zn during Zn^{2+} interaction (**Figure 3**a). The Zn^{2+} intercalation process allows the CTAB-pillared $Ti_3C_2T_x$ to deliver a specific capacity of 86 mAh g^{-1} at 20 mA g^{-1} in 1 M $ZnSO_4$.

The acidity of the electrolyte has a strong impact on the capacity of ZIS in $Ti_3C_2T_x$ MXenes.[115] The charge storage process of $Ti_3C_2T_x$ in different $ZnCl_2$ concentrations has been systematically investigated. Higher $ZnCl_2$ concentrations result in a significant enhancement of the acidity since protons evolve from the solvation shell of complex $ZnCl_4^{2-}$ and $Zn(H_2O)_6^{2+}$ species, which exist in concentrated $ZnCl_2$ solutions. These protons contribute to extra surface redox, leading to an enhanced capacity of 60 mAh g^{-1} in 7 M $ZnCl_2$ compared to 46 mAh g^{-1} in 1 M $ZnCl_2$.

The performance of Nb_2CT_x cathodes was explored in a 21 M LiTFSI/1 M $Zn(OTF)_2$ electrolyte.[60] The authors found that repeated scanning of Nb_2CT_x/Zn at a high voltage of up to 2.4 V could trigger a battery behavior as evidenced by a gradual appearance of a discharge voltage plateau at 1.55 V (Figure 3b). The corresponding electrochemical behavior progressively evolves from capacitive-dominated to diffusion-controlled. Due to the battery-like behavior, an energy density of up to 146.7 Wh kg^{-1} has been achieved, in which around 63% is contributed by the battery plateau. Besides, a stable discharge capacity of 121 mAh g^{-1} at 1 A g^{-1} (95% retention) is obtained over 1800 cycles (Figure 3c). It is noted that the use of water-in-salts electrolytes allows one to set the upper voltage limit of Nb_2CT_x/Zn battery to 2.4 V. At this high voltage, Zn^{2+} ions gain sufficient driving force to insert/extract between the MXene layers.

Compared with $Ti_3C_2T_x$ and Nb_2CT_x, V_2CT_x is less stable and easier to be oxidized in aqueous electrolytes.[116] Taking advantage of this property, V_2CT_x can gradually transform to V_2O_5 during continuous cycling in Zn-based aqueous electrolytes (Figure 3d).[114] Since both V_2CT_x and V_2O_5 contribute to the capacity, a high specific capacity of 508 mAh g^{-1} at 0.2 A g^{-1} and a high energy density of 386.2 Wh kg^{-1} after 18000 cycles have been achieved (Figure 3e). It is worth noting that an excellent rate performance of 200 mAh g^{-1} at a high current density of 10 A g^{-1} can be achieved as well.[114] In another work, a V_2CT_x electrode was synthesized by in-situ electrochemical etching of V_2AlC MAX phase in a fluorine-containing 21 M LiTFSI/1 M $Zn(OTF)_2$ electrolyte.[117] During cycling, the Al layer in the pristine V_2AlC MAX was gradually etched by F^-, forming delaminated V_2CT_x layers. The as-formed V_2CT_x can be further transformed into V_2O_5, which leads to an enhanced capacity of 410 mAh g^{-1} over 1500 cycles and a shift of redox peaks from 0.6 to 0.9 V.

The ZIS performance of MXenes hybrids and high high-entropy alloy MXenes have also been explored. A $Mo_{1.33}CT_x/Ti_3C_2T_x$ free-standing film has been constructed by vacuum-assisted filtrating a $Mo_{1.33}CT_x$-$Ti_3C_2T_x$ (mass ra-

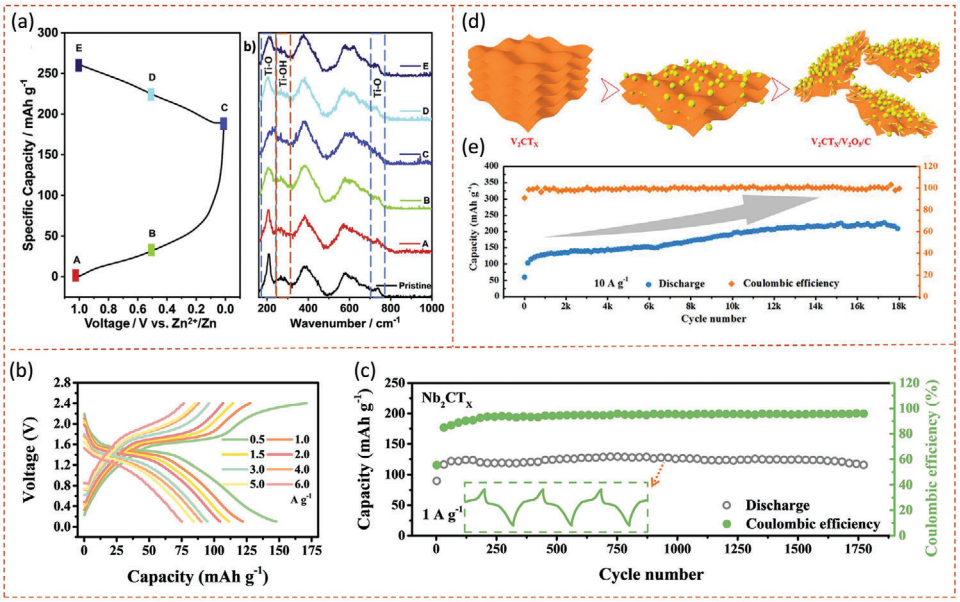

Figure 3. a) Ex-situ Raman spectroscopy data of the in-situ pillared Ti_3C_2. Reproduced with permission.[113] Copyright 2020, Elsevier. b) Galvanostatic charge and discharge at different current densities and c) Long cycling performance of Nb_2CT_x cathode at 1 A g^{-1}. Reproduced with permission.[60] Copyright 2021, Elsevier. d) Schematic diagram of phase structural and phase transition e) long cycling performance of V_2CT_x cathode 10 A g^{-1}. Reproduced with permission.[114] Copyright 2020, American Chemical Society.

tio 3:1) mixture solution.[118] The mixed film shows a higher electronic conductivity than $Mo_{1.33}CT_x$ and a less compact structure (i.e., larger interlayer spacing) than $Ti_3C_2T_x$ in 3 M $Zn(OTF)_2$. Together, this leads to an increased specific capacity of 159 and 59 mAh g^{-1} at a scan rate of 5 and 100 mV s^{-1}, respectively. The successful synthesis of high-entropy MXene, in which several transition metal components are randomly distributed in the M layer of the MXene, creates more possibilities to tailor MXene's electrochemical, catalytic, electrical, and magnetic properties for desired applications.[119] A high-entropy $Ti_{1.1}V_{0.7}Cr_xNb_{1.0}Ta_{0.6}C_3T_x$ film was prepared and its potential for ZIS was tested in 3 M $Zn(OTF)_2$.[120] The film delivers a specific capacity of 77 mAh g^{-1} at 0.5 A g^{-1} and a capacity retention of 87% after 10000 cycles.

3.2. Interfacial Modification of MXenes for Enhanced Zn^{2+} Intercalation

As a pseudocapacitive-type cathode for ZIS storage, the electrochemical properties of MXenes are highly dependent on their interfacial structure, including the interlayer structure and the surface chemistry.[121] Rich surface terminations of the MXene also enable facile construction of MXene-based heterostructures with other nanomaterials. In this regard, different interfacial modification methods exploited for enhancing the ZIS performance will be discussed.

3.2.1. Interlayer spacing regulation

Due to the van der Waals force between 2D MXene flakes, single-layer or few-layer MXene sheets tend to restack together and form a loosely packed multi-layered structure. The stacked MXene layers reduce ion accessibility and prevent rapid ion diffusion between 2D interfaces. Cations (including, Li^+, Mg^{2+}, Al^{3+}, Sn^{4+}) and organic molecules (including, acetonitrile (ACN), dimethyl sulfoxide (DMSO), CTAB, N, N-dimethylacetamide (DMAC)) can be spontaneously inserted as spacers to enlarge the interlayer spacing and address the restacking issue of MXene sheets.[53,113,122,123] For example, a Sn^{4+} pre-intercalated Ti_2CT_x/carbon sphere (Ti_2CT_x/C) electrode was prepared by immersing HF-etched Ti_2CT_x/C in a $SnCl_2$ solution (**Figure 4**a).[53] The Sn^{4+}intercalation enlarges the interlayer spacing of the Ti_2CT_x flakes from 1.15 to 1.27 nm (Figure 4b). Thus, the ion conductivity of Sn^{4+}-Ti_2CT_x/C increases by at least two orders of magnitude as compared to pristine Ti_2CT_x/C due to the expanded ion diffusion channel. The synthesized Sn^{4+}-Ti_2CT_x/C exhibits a prolonged lifespan of 12500 cycles with minimal capacity fluctuation in the 21 M LiTFSI/1 M $Zn(OTF)_2$ electrolyte.

Recently, a variety of fatty diamines and aromatic diamines with different molecular sizes have been employed as pillars to address the restacking of the MXene layer through a one-step amination process.[124] These pillars interact with the =O terminations on the MXene surface and induce a cross-linking assembly with the MXene layer. The molecular size of the diamines has an impact on the interlayer spacing. Among these diamine molecules, p-phenylenediamine (PDA) shows the best performance. The addition of PDA triggers an increase in the $Ti_3C_2T_x$ interlayer spacing from 1.23 to 1.38 nm. A specific capacitance of 124.4 F g^{-1} can be obtained at 0.2 A g^{-1} for PDA-$Ti_3C_2T_x$ in 2 M $ZnSO_4$ electrolytes, along with good cycling stability as highlighted by 85% capacitance retention at 1 A g^{-1} after 10000 cycles.

The facile in-situ insertion of CTAB pillars into MXene flakes can be achieved by introducing 0.1 wt% of CTAB into the 0.1 M $ZnSO_4$ electrolyte.[113] When soaking MXenes in the electrolyte,

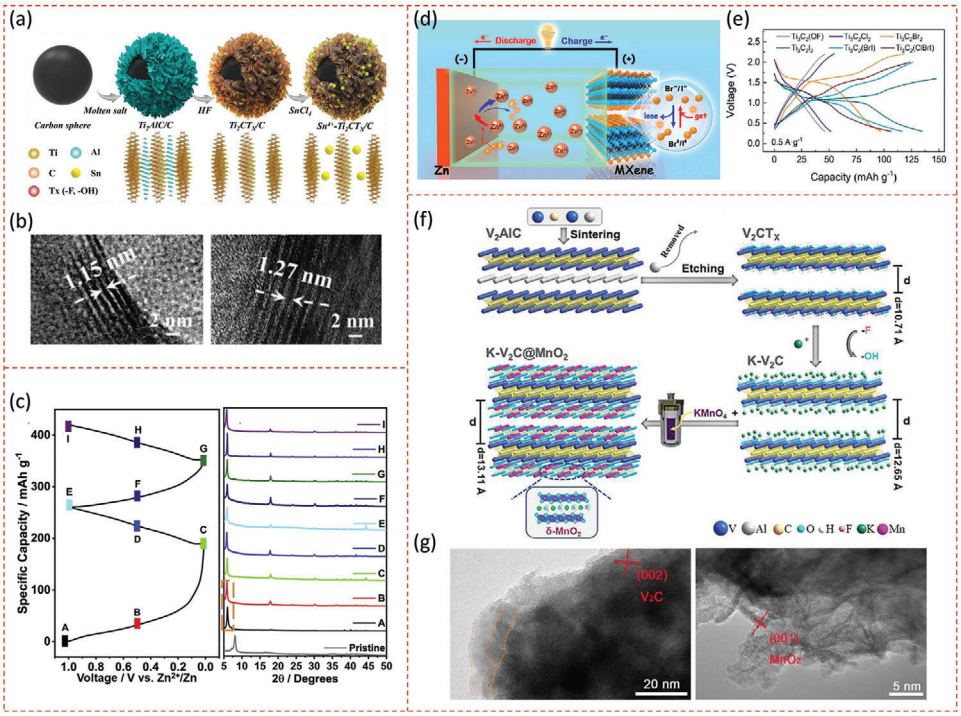

Figure 4. a) Schematic illustration and b) HRTEM images of core-shell sphere Sn^{4+}-Ti_2CT_x/C before and after Sn^{4+} intercalation. Reproduced with permission.[53] Copyright 2020, Wiley-VCH GmbH. c) Ex-situ XRD data of the in-situ pillared $Ti_3C_2T_x$ at different states of charge. Reproduced with permission.[113] Copyright 2020, Elsevier. d) Schematic illustration of Zn^{2+} storage in Cl/Br terminated Ti_3C_2. e) GCD curves of Ti_3C_2 MXenes with different termination groups. Reproduced with permission.[54] Copyright 2021, American Chemical Society. f) Schematic of K^+-V_2CT_x decorated by MnO_2 via template effect and in-situ growth processes. g) High-resolution Transmission Electronic microscopy of K^+-V_2CT_x@MnO_2. Reproduced with permission.[61] Copyright 2021, American Chemical Society.

CTA^+ intercalates into $Ti_3C_2T_x$ to form a stable interlayer spacing for further Zn^{2+} intercalation. The successful introduction of the CTAB and increase in interlayer spacing are confirmed by the enlarged d-spacing as observed by XRD that increases from 1.1 to 1.5 nm at the open circuit voltage. No interlayer spacing change was observed by XRD during (dis)charge, which implies negligible volume change during cycling (Figure 4c). Consequently, the in-situ pillaring of CTAB not only facilitates the transport of Zn^{2+}, but also enhances the structural integrity of MXenes during cycling.

3.2.2. Surface groups modification

The surface groups of MXenes can be modified by changing the synthesis methods or by applying various post-treatment methods. For instance, fluorine-free MXenes can be obtained using molten salt etching in which the A atoms in the MAX phase are oxidized by the cations of the Lewis acid molten salt.[125,126] Meanwhile, the halogen-based anions in the Lewis acid salt attach to the surface of as-synthesized MXenes and become functional groups. The surface groups of the Br-terminated MXene can be further substituted with other groups, including the oxygen, sulfur, selenium, tellurium and NH groups, by exchange reactions.[127]

Well-designed functional groups can boost the ZIS capacity of MXenes. For example, a capacity increase has been reported by introducing redox-active surface groups like –Br and –I through molten salt methods (Figure 4d).[54] Unlike Ti_3C_2OF or $Ti_3C_2Cl_2$, which shows a sloping feature in the galvanostatic charge and discharge curve, the curves of $Ti_3C_2Br_2$ and $Ti_3C_2I_2$ exhibit the discharge plateau at 1.6 and 1.1 V in 21 M LiTFSI/7 M LiOTF/1 M $Zn(OTF)_2$ electrolyte, respectively (Figure 4e). The distinct flat plateau is attributed to the reversible redox reaction of –Br or –I termination, which leads to a substantially enhanced capacity of 97.6 mAh g^{-1} for $Ti_3C_2Br_2$ and 135 mAh g^{-1} for $Ti_3C_2I_2$ at 0.5 A g^{-1}, while a much lower capacity of 46.5 mAh g^{-1} is obtained for $Ti_3C_2Cl_2$. The influence of mixing termination groups is investigated by comparing the performance of Ti_3C_2(BrI) and Ti_3C_2(ClBrI). Although both compositions show dual discharge platforms of Zn^{2+} intercalation, which is attributed to the different redox potential of –Br and –I, Ti_3C_2(ClBrI) delivers a slightly lower specific capacity of 107.4 mAh g^{-1} than Ti_3C_2(BrI) (117.2 mAh g^{-1}) due to its inactive –Cl termination. By optimizing the electrolyte with Cl^- or F^- additives, like 1 M KCl, an additional redox reaction belonging to I_0/I^+ can be activated that can further enhance the capacity of $Ti_3C_2I_2$.[128] The additional Br^- or I^- based redox reaction can also be introduced by electrochemical oxidation and deposition of Br^- or I^- into the interlayer of MXene.[129,130] In this case, the Br_2/I_2 species are confined between the MXene interlayers, eliminating the shuttling effect. Additionally, MXenes with high electronic conductivity and large interlayer spacing also function as a conductive framework for rapid electron and ion transport. Hence, the Br_2-$Ti_3C_2T_x$//Zn

and I_2-Nb_2CT_x//Zn devices show superior rate and cycling stability in the 21 M LiTFSI/7 M LiOTF/1 M Zn(OTF)$_2$ electrolyte.

3.2.3. MXene-based hybrid structures

Although MXene-based cathodes can realize the high-rate capability and long cycle life, the specific capacity of MXene-based cathodes is still moderate for ZIS due to the pseudocapacitive charge storage. Designing MXene-based hybrid structures with other materials, which have a high redox contribution in ZIS, including transition metal oxides or transition metal dichalcogenides, can significantly improve the capacity.[131–135] Meanwhile, the MXene offers a high electronic conductivity to the structure, which guarantees a good rate capability. MXene-based hybrid structures can be formed either by the in-situ transformation of MXenes or by directly mixing MXenes with specific nanomaterials.

Taking advantage of the moderate stability of V_2CT_x, the heterostructure between V_2CT_x and V-based oxides can be constructed by facile hydrothermal methods. A VO_2@V_2CT_x 1D/2D heterostructure was formed in-situ through the partial oxidation of V_2CT_x during a harsh hydrothermal-etching process at 90 °C.[136] The MXene-oxides hybrid structure shows a high capacity of 331 mAh g^{-1} at 5 A g^{-1} in a 3 M Zn(OTF)$_2$ electrolyte. Pre-intercalation of Zn^{2+} can further enhance the rate capability of the MXene-oxides hybrid structure. For example, a V_2CT_x-$Zn_xV_2O_5{\cdot}nH_2O$ (ZVO) heterostructure was synthesized by NaOH pre-alkalization and subsequent hydrothermal treatment in a $ZnCl_2$ solution.[137] Hydrated Na^+ ions can spontaneously intercalate into V_2CT_x during the alkalization process and subsequently exchange with Zn^{2+}. With the hydrothermal method, Zn^{2+}-intercalated V_2CT_x is then partially oxidized and transformed into ZVO. Owing to the pre-intercalated Zn^{2+} and the unique interfaces between ZVO and the conductive framework composed of the remaining V_2CT_x and carbon layer, the resulting V_2CT_x-$Zn_xV_2O_5{\cdot}nH_2O$ exhibits a superior capacity of 223.9 mA h g^{-1} at a high current density of 10 A g^{-1} with ~96.4% capacity retention over 8000 cycles. MXene-dichalcogenides hybrid structures have also been designed to enhance the overall ZIS performance of V-based MXene. For example, through the in-situ selenization of V_2CT_x, the surface layer of V_2CT_x can be transformed into VSe_2, forming a VSe_2@V_2CT_x hybrid structure.[138] This one-step selenization strategy is also applicable for synthesizing $TiSe_2$@$Ti_3C_2T_x$ and $NbSe_2$@Nb_2CT_x. The MXene-dichalcogenides hybrid forms a unique heterogeneous interface, which allows the hybrids to deliver a high-rate capability and a relatively high capacity retention of 93.1% after 600 cycles.

It has been reported that MXenes not only act as the conductive framework for electron and ion transport, but also minimize the volume expansion/contraction during cycling. On top of that, it has been shown that MXene hybrids can inhibit the irreversible dissolution of Mn-based materials in the electrolyte during cycling (see Section 2.1). A K^+ pre-intercalated V_2CT_x@MnO_2 hybrid material, in which MnO_2 nanosheets are uniformly attached to the V_2CT_x MXene surface, has been designed and investigated as a cathode for ZIS (Figure 4f).[61] XRD results of K-V_2CT_x@MnO_2 electrodes show no phase change after cycling, which demonstrates its excellent structural stability, while new crystalline phases of MnO and MnOOH were observed in pure δ-MnO_2 electrodes. As a result, K-V_2CT_x@MnO_2 delivered a high specific capacity of 408.1 mA h g^{-1} at 0.3 A g^{-1}, which exceeded most of the Mn-based and MXene-based cathodes reported so far. In addition, a superior cycling performance without an obvious capacity decay after 10000 cycles was achieved.

4. MXenes in the ZIS Anodes

Free-standing $Ti_3C_2T_x$ MXene films can be used as negative electrodes (or anodes) for aqueous ZIS when paired with cathodes with higher Zn intercalation potentials.[139] However, the $Ti_3C_2T_x$ negative electrode only has a moderate charge storage capability compared to the Zn metal anode, as the capacitive behavior dominates the charge storage process of MXenes. Instead, the merit of MXenes on the anode side is their ability to modify the Zn metal anode-electrolyte interface to assist the Zn deposition/stripping and suppress the side reactions. Table S2 summarizes recent applications of MXenes as interfacial materials to modify the Zn anode and separator, as well as electrolyte additives to induce uniform nucleation and inhibit dendrites. Thereby, MXenes have become one of the most promising interfacial layers between the Zn metal and aqueous electrolyte by virtue of their zincophilic nature, remarkably high conductivity, and easy solution processing.

4.1. Anode Surface Modification with A MXene Layer

Coating the Zn anode with a protective layer can shield it from directly contacting the aqueous electrolyte, thus reducing the occurrence of side reactions. Given the zincophilic, hydrophilic and highly conductive properties of MXenes, modification of Zn anodes with MXene sheets endows the Zn anode with a much lower Zn nucleation energy barrier and more uniform electric field distribution. For example, a facile in-situ spontaneous reducing/assembling strategy has been developed to assemble MXene nanosheets on the surface of the Zn anode (**Figure 5**a).[28] The introduction of the MXene as an artificial interface layer homogenizes the electric field distribution (Figure 5b,c) and reduces the Zn nucleation potential barrier (Figure 5d). Hence, the Zn dendrite growth is effectively suppressed on the MXene-coated Zn anode, and a ZIS device built with this anode exhibits good cycling stability with 81% capacity retention after 500 cycles.

$Ti_3C_2T_x$ MXene can also be coated on the Zn metal surface by adding MXene as an additive to the $ZnSO_4$ electrolyte.[140] The MXene flakes are in-situ coated on the Zn metal surface by first combining with Zn^{2+} via electrostatic interactions and then adsorption on the Zn surface, forming an optimized electrode/electrolyte interface. Notably, compared with Zn foil, $Ti_3C_2T_x$ displays better affinity with atomic Zn via the =O group (Figure 5e,f), and Zn^{2+} ions have already dispersed well on the MXene surface before being deposited on the Zn surface. In this way, the dispersed Zn-ions function as seed points, inducing uniform nucleation and further inhibiting dendrites.

Zn powder anodes possess distinct advantages over Zn foil anodes due to their low cost, excellent processability, and easy

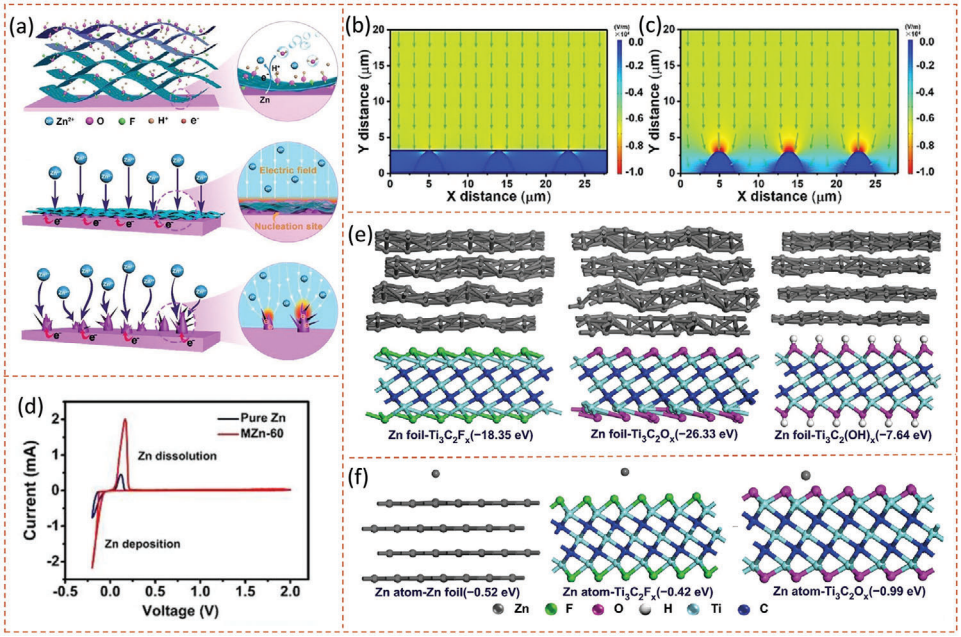

Figure 5. a) Illustration of synchronously reducing and assembling of MXene layers on the surface of Zn foil, Zn plating behavior of MXene-coated Zn and pure Zn. b,c) Models of the electric field distributions for b) MZn-60 and c) pure Zn. d) CV curves of Zn plating/stripping at 0.1 mVs^{-1}. Reproduced with permission.[28] Copyright 2020, Wiley-VCH GmbH. e) $Ti_3C_2T_x$ adsorbed on Zn foil and f) Zn atoms absorbed on Zn foil, $Ti_3C_2T_x$ and the corresponding binding energies. Reproduced with permission.[140] Copyright 2021, Springer Nature.

tunability. The failure of Zn powder anodes is mainly caused by the rapid overpotential deterioration during cycling, which is different from that of Zn foil anodes.[141] In order to prevent rapid electrode failure, $Ti_3C_2T_x$-wrapped Zn powder (MXene@Zn) anodes can be prepared through an electrostatic self-assembly method.[141] In this MXene@Zn anode, the highly conductive 2D $Ti_3C_2T_x$ flakes serve as electron and ion redistributors for uniform Zn^{2+} deposition. Meanwhile, the low lattice mismatch (10%) between the (002) plane of Zn deposits and the Ti surface of $Ti_3C_2T_x$ can potentially facilitate the formation of a coherent heterogeneous interface and hence induce dendrite-free Zn deposition. Accordingly, MXene@Zn anodes show superior deposition thermodynamics, much lower voltage hysteresis and a dramatically reduced overpotential as compared with Zn powder anodes without MXene coatings.

Introducing a large number of N-containing functional groups on MXene-based protective layers can also increase the reversibility of the Zn metal anode. Density functional theory simulations reveal that Zn^{2+} can be strongly adsorbed on the zincophilic nitrogen-containing groups on the MXene sheets, which induces a uniform deposition of Zn along the (002) crystal plane. A facile self-assembly approach is used to prepare a tetramethylammonium intercalated $Ti_3C_2T_x$ MXene, which can be applied as an interfacial protection layer to modify the Zn anode (MX-TMA@Zn) (**Figure 6**a).[51] The charge redistribution over MX-TMA provides a uniform electric field distribution on the Zn anode. Moreover, compared with the Ti_3C_2 and $Ti_3C_2O_y$, the DFT results show that $Ti_3C_2O_y$ doped by quaternary N (N_q) functional group delivers the highest binding energy (−1.89 eV) (Figure 6b), indicating the N functional group has an enhanced ability to capture zinc ions. Additionally, the wettability of the MX-TMA coating with N_q is greatly improved (Figure 6c), and this coating also greatly shortens the 2D diffusion time of zinc ions (Figure 6d), which is conducive to forming a uniform and dense zinc layer and inhibiting the growth of Zn dendrites (Figure 6e). As a result, the MX-TMA@Zn anode demonstrates a long lifespan of 3600 h under 2 mA cm^{-2} and 450 h deep discharge.

The surface groups of MXenes can be halogenated for MXene-based protective layers. A series of stoichiometric halogenated MXenes, including $Ti_3C_2Cl_2$, $Ti_3C_2Br_2$ and $Ti_3C_2I_2$, have been explored as artificial protective layers of the Zn anode.[52] All the halogenated MXene-Zn anodes outperform the bare Zn anode in nucleation overvoltage, Coulombic efficiency, polarization and durability. The outperformance is due to the synergistic effect of high lattice matching (Figure 6f,g) and halogen regulation, contributing to the subsequent oriented Zn growth mode. In terms of Zn^{2+} regulation, −Cl termination is found to be more effective than −O/F, −Br and −I terminations. This is ascribed to the moderate adsorption and diffusion coefficiency for Zn-ions on the MXene with −Cl terminations (Figure 6h). As a result, the $Ti_3C_2Cl_2$-Zn/$Ti_3C_2I_2$ battery can operate over 9000 cycles with a capacity decay rate of only 2.93% per thousand cycles, superior to the Zn//$Ti_3C_2I_2$ battery that features an attenuation rate of 7.95% per thousand cycles.

3D heterogeneous films constructed from MXenes can also function as protective layers. A heterogeneous layer composed of an electronically conductive sulfur-doped 3D MXene skeleton and an ionic conductive ZnS has also been designed to protect a Zn metal anode (S/MX@ZnS@Zn) (**Figure 7**a).[56] S/MX@ZnS@Zn significantly reduces the polarization potential of Zn deposition (Figure 7b) and inhibits the growth of Zn dendrites and side reactions, buffering volume changes and func-

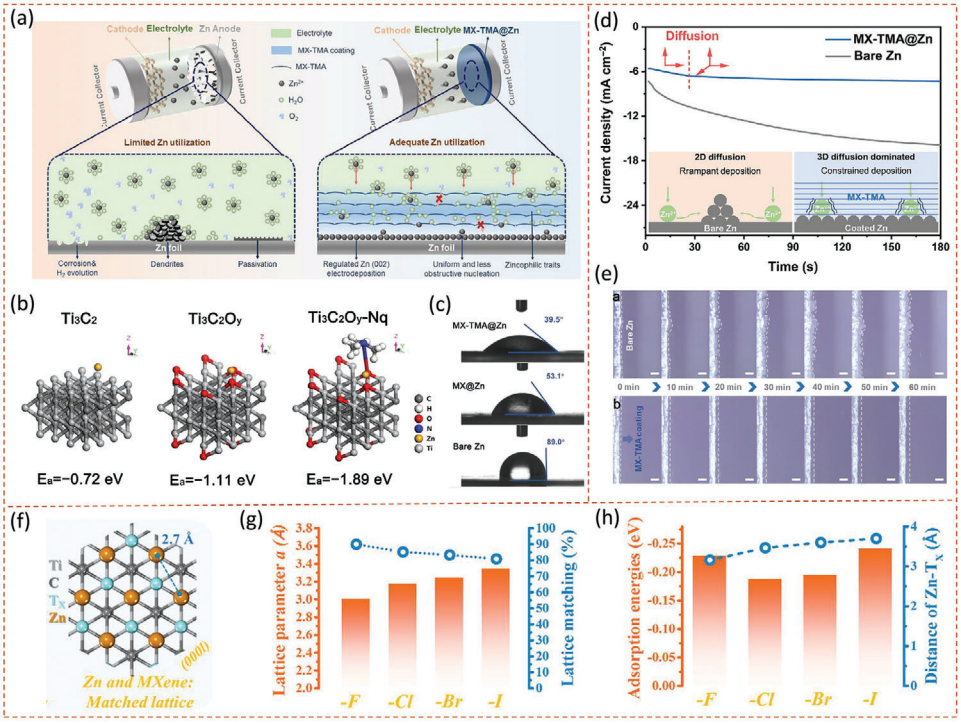

Figure 6. a) Schematic diagram showing zinc deposition behavior on bare Zn and MX-TMA@Zn (To facilitate the reader's understanding, the nucleation position is placed on the zinc substrate. In fact, the nucleation position should be in the MXene skeleton). b) Calculation model of the binding energy of zinc ions adsorbed on different functional groups on MXene substrate. c) Contact angles of the electrolyte on MX-TMA@Zn, MX@Zn, and bare Zn. d) Chronoamperograms of MX-TMA@Zn and bare Zn at a −150 mV overpotential (the insets: the schematic diagram of Zn^{2+} diffusion and reduction process on MX-TMA@Zn electrode and bare Zn electrode, which shows that 2D diffusion is constrained by MX-TMA coating). e) In-situ optical microscope images of the zinc-electrodeposition behavior on bare Zn and MX-TMA@Zn electrodes were observed by symmetrical transparent cells at a current density of 5.0 mA cm^{-2} (scale bars: 100 µm). Reproduced with permission.[51] Copyright 2022, Elsevier. f) Schematic illustration of MXene crystal structure matching Zn deposits on MXene. g) Lattice parameters a versus calculated lattice matching ratios of halogen-terminated $Ti_3C_2(F/Cl/Br/I)_2$. h) Calculated atomic distance between Zn atom and neighboring halogen termination versus calculated adsorption energies of different MXene surfaces to Zn atoms. Reproduced with permission.[52] Copyright 2022, American Chemical Society.

tioning as a physical barrier. Meanwhile, the introduction of highly ionic conductive ZnS ensures a uniform Zn^{2+} distribution and eliminates side reactions. Benefiting from the synergistic effect of the heterogeneous layer, a highly reversible dendrite-free Zn anode is realized, exhibiting a stable cycling performance for up to 1600 h. Similarly, a heterogeneous layer formed with N/Se functionalized MXene nanowire/nanosheet skeleton and ionic conductive ZnSe nanoparticles was also applied as a protective layer for Zn metal anodes (Figure 7c).[142] As a result, a uniform Zn deposition with a low nucleation resistance (Figure 7d) is induced, and interface side reactions are inhibited.

Forming MXene-based heterogeneous films with polymers can introduce additional functions to the protective layer that can further enhance the stability of Zn anodes. A MXene and mesoporous polypyrrole composite film (MXene-mPPy) can be prepared by controllable polymerization of pyrrole on both sides of the MXene. Subsequently, the MXene-mPPy can be coated on the Zn foil by employing a spray-coating technology (Figure 7e).[143] The sandwich-structured film exhibits charge enrichment ability, which favors charge accumulation and homogenizes the dispersions of the electric field and ion flux. Thus, the MXene-mPPy coated Zn anodes show a long cycling lifespan of 2500 h with a dendrite-free morphology. However, in this method, the introduction of hydrogen peroxide, the initiator used for polymerizing PPy may cause partial oxidation of the MXene, resulting in titanium oxide residues in the system. Flexible artificial protective layers composed of MXene nanosheets and chitosan (MX/CS) can also firmly adhere to the Zn foil through facile blade-casting.[144] Benefiting from the abundant amine groups of chitosan, the composite film offers numerous coordination sites for facilely capturing Zn^{2+}, which decreases the concentration gradient of Zn^{2+} near the anode and homogenizes Zn^{2+} flux for uniform nucleation. Consequently, the reversibility of the Zn anode is enhanced, demonstrating a high Coulombic efficiency of 99% in a Zn||Cu asymmetric cell after 500 cycles. MXenes have also been used for assisting the polymer coating on Zn anodes directly from an aqueous monomer solution.[145] A P(AA-co-AMPS) polymer-MXene composite film can be coated on the Zn anode by combining the doctor-blade method with the spontaneous polymerization of monomers. The composite film with strong adhesion and good interfacial contact with the Zn anode suppresses the side reactions and facilitates uniform Zn deposition.

The introduction of MXene-based interfacial materials onto the Zn anode can significantly inhibit the growth of Zn dendrites and side reactions. Compared with ex-situ preparation methods,

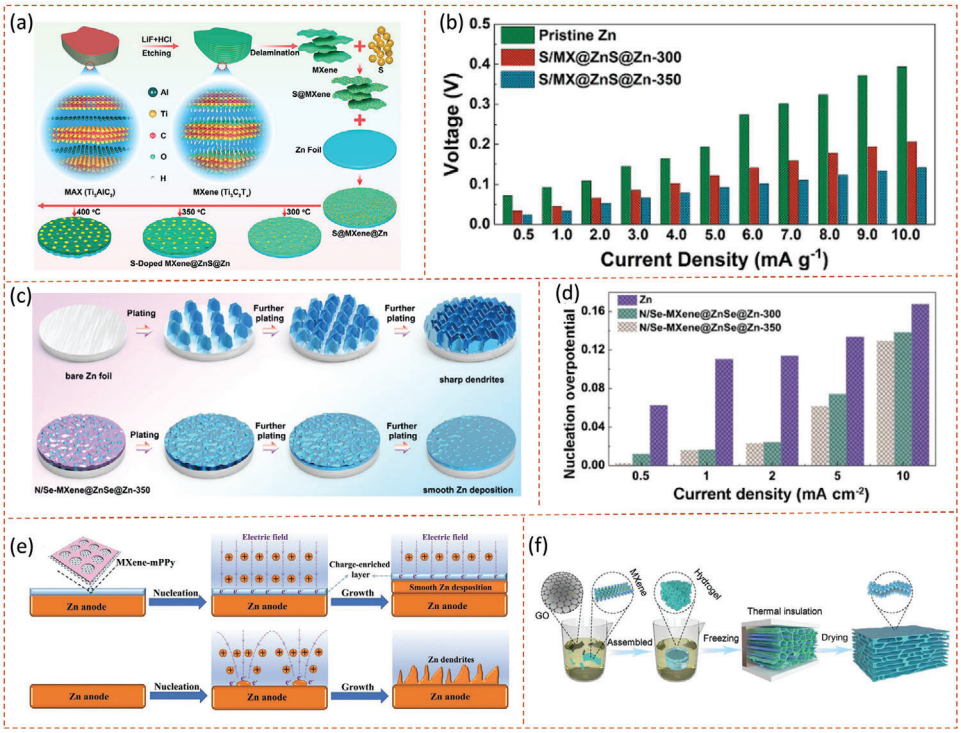

Figure 7. a) Schematic Illustration of Fabrication of S/MX@ZnS@Zn at Different Temperatures. b) voltage hysteresis of pristine Zn and S/MX@ZnS@Zn anodes in aqueous electrolytes at a series of rates. Reproduced with permission.[56] Copyright 2021, American Chemical Society. c) The schematic illustration of Zn deposition behaviors on bare Zn and N/Se-MXene@ZnSe@Zn-350 anodes. d) Nucleation overpotential of Zn, N/Se-MXene@ZnSe@Zn-300, and N/Se-MXene@ZnSe@Zn-350 anodes at different current densities. Reproduced with permission.[142] Copyright 2022, Elsevier. e) Schematic illustrations of the Zn plating behaviors on MXene-mPPy/Zn and bare Zn. Reproduced with permission.[143] Copyright 2022, Wiley-VCH GmbH. f) Schematic illustration of fabricating MGA material. Reproduced with permission.[62] Copyright 2021, Wiley-VCH GmbH.

such as spraying and doctor-blade method, the interface layer generated by in-situ self-assembly has a stronger adhesion to Zn metal and presents more advantages in long cycles. In addition, the mild preparation conditions are advantageous for avoiding the oxidation of MXene and eliminating the potential impurities in the system.

4.2. 3D MXene-Based Frameworks for Zinc Deposition

Anodes with a 3D porous network possess a great number of nucleation sites for ion deposition and abundant channels to facilitate ion flux.[146] MXenes with such a structure allow Zn^{2+} to be plated not only on the external surface of the 3D structure, but also in the interior of the 3D network, which is expected to alleviate volume deformation of the anode and inhibit dendrite formation.[92,147,148] However, the porous structure increases the contact area between the Zn anode and the aqueous electrolyte, which might accelerate Zn corrosion. In order to mitigate the dendrite growth and inhibit the side reactions at the 3D anode interface, a flexible 3D MXene/rGO aerogel can be fabricated through an oriented freezing process (Figure 7f).[62] The zincophilic nature and porous structure of the aerogel allow a dense encapsulation of Zn in the 3D structure. Meanwhile, the −F terminations in the MXene can interact with Zn^{2+} during cycling to form ZnF_2-rich solid electrolyte interphase, which effectively suppresses the dendrite growth and inhibits the direct contact between the electrolyte and the anode. Moreover, Zn distributed in a 3D microscale manner suppresses the passivation reaction and HER during cycling. As a result, a symmetrical cell with MXene/rGO aerogel@Zn electrode exhibits a long lifespan of over 1000 h at 10 mA cm^{-2} with a uniform Zn deposition. Alkalized 3D MXenes with pre-intercalated metal ions can also be used as a framework for Zn deposition.[149] The alkalization and pre-intercalation operation introduces a nanoribbon structure to the framework and avoids the restacking of flakes, which improves the energy storage capacity and efficiency of the anode.

The introduction of the porous structure facilitates the transport of Zn^{2+} ions and increases the number of nucleation sites. Meanwhile, the limited volume units constrain the growth of dendrites and suppress the side reactions. However, the relationship between the porosity and the dendrite growth deserves further exploration.

4.3. MXene in Zn-free Metal Anode Materials

In traditional Zn anodes, the Zn^{2+} plating/stripping process mainly takes place on the external surface of the metal anode, and only a small fraction of the Zn metal (<5%) is actually involved in the electrochemical reaction and contributes to the capacity.[150] Hence, using an excess of Zn metal significantly decreases the

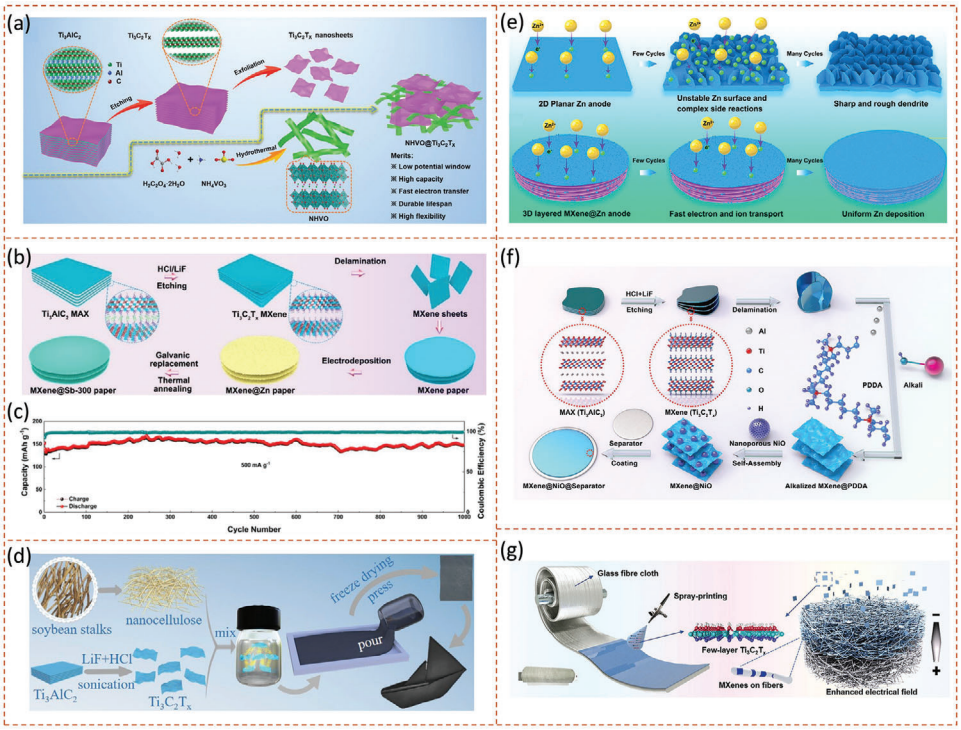

Figure 8. a) Schematic illustration of the preparation process of NHVO@$Ti_3C_2T_x$ electrode. Reproduced with permission.[152] Copyright 2021, Wiley-VCH GmbH. b) Schematic illustration of the fabrication process. c) Long-term cycling performance of MXene@Sb-300 electrode at 500 mA g^{-1}. Reproduced with permission.[154] Copyright 2021, Elsevier. d) Schematic illustration for fabricating the $Ti_3C_2T_x$/nanocellulose hybrid film and photographs of the MN-90 film. Reproduced with permission.[63] Copyright 2022, American Chemical Society. e) Schematic of morphology evolution for bare Zn and $Ti_3C_2T_x$ MXene@Zn anode during the stripping/plating process. Reproduced with permission.[155] Copyright 2019, American Chemical Society. f) Schematic illustration of the synthesis process for the MXene@NiO modified separator. Reproduced with permission.[156] Copyright 2022, American Chemical Society. g) Schematic diagram depicting the preparation and function of MXene-GF separator. Reproduced with permission.[64] Copyright 2022, Wiley-VCH GmbH.

actual volumetric/gravimetric specific energy density of a battery. Similar to the configuration of a commercial Li-ion battery (anode-free Li-metal battery), replacing the Zn metal anode with an intercalation-based anode can potentially improve the full-cell energy density and solve the issue with dendrite growth.[151] For instance, a novel $(NH_4)_2V_{10}O_{25}.8H_2O$@$Ti_3C_2T_x$ thin film anode shows a low Zn^{2+} average discharge potential of 0.59 V (relative to Zn^{2+}/Zn) at 0.1 A g^{-1}.[152] In this anode, the $Ti_3C_2T_x$ not only provides an interconnected conductive network, but also stabilizes the $(NH_4)_2V_{10}O_{25}.8H_2O$ nanobelts structure (**Figure 8**a). When pairing the anode with a $ZnMn_2O_4$ cathode, a "rocking-chair" battery can be constructed, providing a high capacity of 131.7 mAh g^{-1}, a maximum energy density of 97.1 Wh kg^{-1}, and a high capacity retention of 92.1% after 6000 cycles. Recently, a "rocking-chair" Zn-ion micro-battery was constructed by adopting a free-standing MXene-TiS_2 as an anode, MWCNTs-VO_2(B) as a cathode, and $ZnSO_4$-polyacrylamide as a hydrogel electrolyte.[153] This micro-battery exhibits a specific capacity of 40.8 μAh cm^{-2}, a maximum energy density of 1.2 mWh cm^{-2}, along with good flexibility and self-healability.

Although intercalation-based anodes effectively suppress Zn dendrite growth and harmful side reactions, the intercalation potential of such anode is usually much more positive than that of Zn metal, which reduces the working voltage window of the battery. Additionally, the specific capacity associated with the intercalation of the active electrode material is relatively lower than Zn deposition. Hence, it is appealing to realize a highly reversible plating/striping energy storage process on a Zn-free anode.[63,154,157–159] $Ti_3C_2T_x$ MXene films are able to assist the reversible Zn plating/striping, as the presence of MXene makes the deposited Zn more prone to form thin hexagonal flakes that are horizontal to the film surface. That is because the low lattice mismatch between the $Ti_3C_2T_x$ surface and the (002) facet of Zn promotes the growth of the deposited Zn along the (002) plane.[63]

Further modification of MXenes with functional nanomaterials can boost the reversibility of the MXene-based alloying-type Zn-free anodes. Antimony (Sb) nanoarrays modified 3D $Ti_3C_2T_x$ MXene paper can serve as an alloying-type anode.[154] The MXene@Sb anode can be prepared by electrodepositing Zn on the MXene, followed by a replacement reaction with $SnCl_3$ (Figure 8b). Zn can reversibly alloy with Sb to form ZnSb, realizing an alloying-type ZIS. Meanwhile, the zincophilic Sb nucleation seed and 3D structure of the MXene can regulate homogeneous Zn deposition. Consequently, the $Ti_3C_2T_x$ MXene@Sb anode harvests a long cycling life of up to 1000 cycles with a high average Coulombic efficiency of 97.2% (Figure 8c). An aqueous "rocking-chair" made from the MXene@Sb anode and the $ZnMn_2O_4$ cathode delivers a high capacity of 120 mAh g^{-1} at 200 mA g^{-1} and sustains a stable cycling performance over 100 cycles. Alternatively, a nanocellulose-modified $Ti_3C_2T_x$ hybrid film, which is

prepared by a solution casting method (Figure 8d), is applied as a Zn-free anode.[63] The hydroxyl groups on the nanocellulose possess strong interactions with Zn^{2+}, preventing the unfavorable Zn^{2+} transport along the anode surface and hence suppressing the Zn dendrite growth. Meanwhile, the hydroxyl group can also promote the desolvation of the hydrated Zn^{2+} through hydrogen bonds. By combining the nanocellulose with MXene, the mechanical properties, electrical conductivity, and electrolyte wettability of the electrode are also improved. To demonstrate the advantage of nanocellulose-MXene anodes, a flexible quasi-solid-state Zn-Li hybrid battery can be assembled, exhibiting a high capacity retention of 82% after 2000 cycles. Another work reports the fabrication of an ultrathin Zn-free anode of only 6.2 μm by coating the $Ti_3C_2T_x$/nanocellulose composite on a stainless steel foil.[159] Similarly, the anode shows improved Zn plating kinetics, lower nucleation overpotential and suppressed side reactions, and delivers a good rate capability and long cycling life when assembled in a hybrid Zn-Na battery.

5. MXenes in Substrates and Separators

Although substrates and separators are not capacitance/capacity-contributing components, they can substantially influence the performance of ZIS devices by regulating electron and ion transport to/from the anode. With an ultrahigh electronic conductivity, $Ti_3C_2T_x$ films have shown promising performances when served as a substrate for Zn anodes. A Zn@$Ti_3C_2T_x$ anode can be created by electrochemical deposition of 3D Zn nanoflakes on a $Ti_3C_2T_x$ substrate.[112] The highly conductive $Ti_3C_2T_x$ substrate enables a fast electron transfer at the Zn/$Ti_3C_2T_x$ interfaces, ensuring a high-rate electrochemical reaction. Similarly, a $Ti_3C_2T_x$ MXene@Zn paper, fabricated by in-situ electroplating Zn on a $Ti_3C_2T_x$ MXene film in $ZnSO_4$ electrolyte (Figure 8e), shows a suppressed dendrite growth when used as an anode.[155] In this case, the improved performance is attributed to the MXene substrate, which provides a highly conductive, hydrophilic, and compatible interface for the Zn deposition. Moreover, Zn/MXene films prepared by in-situ electroplating have a strong Zn-MXene interface and excellent mechanical flexibility, enabling its application in flexible ZIBs.[132]

When MXenes are used as regulators for separators, their surface groups can functionalize the separator-electrolyte interface to influence the flow of Zn-ions. A series of MXene-oxide (CoO, CuO, MgO, In_2O_3, TiO_2, etc.) heterostructures can be prepared by a one-step vacuum distillation technique which can be used for decorating the separators in aqueous ZIBs (Figure 8f).[156] It was found that zincophilic heterostructures can homogenize the electric field distribution, enhance the ion transport kinetics by reducing the Zn^{2+} concentration gradient, and minimize the overpotential of Zn deposition. The lower overpotential assists the uniform Zn deposition and suppresses side reactions. As a result, the Zn anode can be operated up to 500 h under high operating current (10 mA cm^{-2}) and area capacity (10 mAh cm^{-2}).

A Janus $Ti_3C_2T_x$-decorated glass fiber separator can be fabricated by spray-printing MXene nanosheets over one side of a commercial glass fiber (Figure 8g).[64] Apart from sufficient surface polar groups, good electrolyte wettability, and high ion conductivity, the MXene-glass fiber also exhibits a higher dielectric constant than pristine MXenes. These properties help to construct a directional built-in electrical field via the Maxwell-Wagner effect to expedite Zn^{2+} migration. On the other hand, the abundant surface groups of the MXene lower the desolvation energy, promotes Zn^{2+} diffusion, facilitate the uniform deposition of Zn metal, and minimize corrosion reactions. With the separator, a symmetric cell harvests an elongated cycle life of 1180 h at 1 mA cm^{-2} and 1 mAh cm^{-2}. A full battery assembled with $KV_{12}O_{30-y}\cdot nH_2O$ as the cathode and Zn plate as the anode can retain 77.9% capacity upon cycling at 5 A g^{-1} for 1000 cycles.

While separators decorated with $Ti_3C_2T_x$ and $Ti_3C_2T_x$ electrolyte additives have demonstrated remarkable positive effects on Zn ion transport, suppression of dendrites and side reactions, the impact of other MXenes on the performance of ZIS still remains unclear. Moreover, with respect to the high electronic conductivity of MXenes, their contents in the separator and electrolyte should be well controlled to avoid short circuit of the system.

6. Summary and Perspectives

In summary, aqueous ZIS devices have been considered as one of the competitive energy storage devices for future large-scale electrical energy storage applications in view of their environmental benignity, intrinsic safety, and high energy density. Featuring a large specific surface area, extremely high conductivity, and rich surface chemistry, 2D MXenes have shown great potential in boosting the overall performances of ZIS. In this review, we summarized the latest progress on the interfacial design of 2D MXenes for enhancing the performance of ZIS. First, the importance of the interfaces was demonstrated by summarizing the charge storage mechanism and electrochemical reactions/processes of typical ZIS cathode and anode materials. Then, we showed that the modification of MXene interfacial properties (including interlayer space, surface groups and hybrid interfaces) could increase the Zn storage capability, high-rate performance and cycling stability of MXene-based cathodes. On the anode side, we focused on the application of MXenes as the interface between the Zn metal electrode and electrolyte to facilitate Zn deposition, suppress dendrites and prevent side reactions. Specifically, MXenes can be used as protective layers, offer 3D frameworks for Zn deposition and function as Zn-free anodes. Finally, we discussed that the utilization of MXene in the substrates and separators can further improve the ZIS performance by facilitating ion and electron transport.

Despite intensive efforts and considerable progress to date, aqueous MXene-based ZIBs and ZICs with sufficiently high energy density while maintaining high power density and long lifespan are yet realized for large-scale energy-storage applications. To this end, a number of challenges need to be addressed in future investigations.

Applications of MXenes in ZIS heavily rely on the cost-effective routes for large-scale production of MXenes. Although hundreds of MXenes have been theoretically predicted, current research still mostly focus on the Ti and V-based MXenes. Deeply understanding the interfacial structure and surface chemistry of other MXene families would bring broad opportunities for MXene-based 2D materials in ZIS. Besides, the synthesis of MXenes by conventional wet chemistries usually involves the etching of A atoms from MAX phases with HF solution or a LiF and HCl mix-

ture, which is dangerous and environmentally hazardous. Consequently, green and cost-effective routes for scalable production of MXenes are urgently required for their practical applications.

Charge-storage mechanism of MXene-based ZIBs and ZICs needs in-depth understanding. The use of advanced in-situ characterization techniques, such as in-situ transmission electron microscopy, diffraction and spectroscopic characterization will help us to probe the structural changes of M members and surface functional groups T_x of MXenes at the electrode/electrolyte interfaces. The real-time monitoring of morphology changes and the compositional and structural evolution of electrodes during the charging/discharging process are crucial to deeply understanding the interfacial reaction mechanisms and will provide constructive and general guidelines for the future design of novel electrodes. On the other hand, with the assistance of computational simulation, the bonding length, binding energy and favorable binding position at Zn^{2+} and MXenes interfaces can be precisely predicted, which provides important insights into the charge storage mechanism at the atomic-level.

Dendrite growth and side reactions of Zn anodes seriously threaten the lifespan of both aqueous ZIBs and ZICs. Recent achievements have shown that the growth of Zn dendrites at low current density had been strongly suppressed with the assistance of MXenes. However, the Zn dendrite issue and low Coulombic efficiency at a fast charging/discharging rate still remain a big challenge. With remarkable zincophilicity and good chemical compatibility, MXene artificial interlayers with regulated surface terminations to get an improved lattice matching is conductive to the formation of coherent heterogeneous interfaces between the (002) plane of deposited Zn and (002) plane of MXene. On the other hand, constructing MXene-based 3D spatial structures not only promotes fast Zn^{2+} ion transport, but also reduces the local charge accumulation and improves the Coulombic efficiency of Zn deposition/stripping. In this regard, pore structure of the MXene-based artificial interlayers needs to be optimized and their size effects on the zinc dendrite growth require further understanding.

Exploring new electrolytes. Aqueous electrolytes offer distinct advantages over organic electrolytes in light of their much higher ion conductivity, environmental benignity and operating safety. These properties render the aqueous-based ZIBs or ZICs fast ion kinetics and very high power density. However, the solvation structure of zinc ions, itself depending on the solvents, the added additives and the concentration of zinc salt, fundamentally affects the electrochemical stability, operating voltage window and the deposition/stripping efficiency of zinc anodes. Comprehensively understanding of the coordination circumstances of zinc ions would benefit the design of aqueous electrolyte systems. Besides, other aspects like the cost and compatibility with the electrode should also be taken into consideration. Meanwhile, polymer-based gel electrolytes possessing superior mechanical flexibility are important for flexible device construction. In this regard, good anti-freezing properties and high zinc ion conductivity are of special importance for full-temperature flexible quasi-solid-state ZIBs and ZICs devices. Besides, the compatibility of the polymer-based gel electrolytes with the electrodes should also be considered to minimize the interfacial barrier of ionic transport.

Design of flexible electrodes for ZIB and ZIC devices. While recent years have witnessed tremendous research advances in the field of aqueous ZIBs and ZICs, there is still a long way to go before their large-scale commercial application. The fast growth of the market for various stretchable electronic systems and smart wearable electronic products may expedite the development of ZIBs and ZICs as light, thin, flexible and stretchable storage devices. In order to simultaneously fulfill charging and flexible functions, both cathodes and anodes should have sufficient flexibility for device bending and/or stretching. For the cathodes, flexible MXene electrodes with enlarged interlayer spacing could facilitate Zn^{2+} insertion and maximize the electrochemical performance. On the other hand, placing electroactive cathodes between MXene interlayers to construct MXene-based hybrid materials is also an attractive method to improve the performance of cathodes. In this regard, the specific capacity of active cathodes, the conductivity and mechanical flexibility of the whole cathodes should be well balanced to achieve optimized performance. In particular, strong interfacial interactions between the conductive MXenes and active cathodes deserve more attention as such structures can greatly minimize the interfacial resistances, which contribute to a high-rate performance by accelerating the electron transports across the interfaces. On the anodes side, flexible Zn-free anodes capable of reversibly stripping/plating of Zn with a high Coulombic efficiency is highly desirable as the use of Zn-free anodes can maximize the device's energy density. Porous MXenes with large surface area and favorable ion pathways are promising Zn-free flexible anodes as exemplified by their outstanding conductivity, good flexibility and remarkable zincophilicity.

Supporting Information

Supporting Information is available from the Wiley Online Library or from the author.

Acknowledgements

R.G. and C.C. contributed equally to this work. This work was supported by the Dutch Research Council (NWO) under Open Competition Domain Science XS (OCENW.XS22.3.009). The authors R.G., C.C. and H.W. are grateful for the fellowship from the China Scholarship Council (202106870046, 202106170009, and 202206630042). Z.S. was supported by ERC-CZ program (project LL2101) from Ministry of Education Youth and Sports (MEYS). This work was also supported by the National Natural Science Foundation of China (No. 51772181), 111 project (B14041), the Natural Science Basic Research Plan of Shaanxi Province (No. 2019JLP-12), and Shaanxi Sanqin Scholars Innovation Team.

Conflict of Interest

The authors declare no conflict of interest.

Keywords

2D MXenes, interfacial design, mild aqueous electrolyte, Zn-ion batteries, Zn-ion capacitors

Received: December 20, 2022
Revised: February 16, 2023
Published online:

[1] Y. Ding, P. Cai, Z. Wen, *Chem. Soc. Rev.* **2021**, *50*, 1495.
[2] B. Steffen, F. Egli, M. Pahle, T. S. Schmidt, *Joule* **2020**, *4*, 1137.
[3] B. Obama, *Science* **2017**, *355*, 126.
[4] V. Viswanathan, A. H. Epstein, Y. M. Chiang, E. Takeuchi, M. Bradley, J. Langford, M. Winter, *Nature* **2022**, *601*, 519.
[5] H. Xue, H. Gong, Y. Yamauchi, T. Sasaki, R. Ma, *Nano Res. Energy* **2022**, *1*, e9120007.
[6] M. V. Reddy, A. Mauger, C. M. Julien, A. Paolella, K. Zaghib, *Materials* **2020**, *13*, 1884.
[7] R. Zhan, X. Wang, Z. Chen, Z. W. Seh, L. Wang, Y. Sun, *Adv. Energy Mater.* **2021**, *11*, 2101565.
[8] M. Piglowska, B. Kurc, M. Galinski, P. Fuc, M. Kaminska, N. Szymlet, P. Daszkiewicz, *Materials* **2021**, *14*, 6783.
[9] C. M. Costa, J. C. Barbosa, R. Gonçalves, H. Castro, F. J. D. Campo, S. Lanceros-Méndez, *Energy Storage Mater.* **2021**, *37*, 433.
[10] C. Zhang, F. Wang, J. Han, S. Bai, J. Tan, J. Liu, F. Li, *Small Struct.* **2021**, *2*, 2100009.
[11] U. Fegade, G. Jethave, F. Khan, A. Al-Ahmed, R. Karmouch, M. Shariq, Inamuddin, M. F. Ahmer, *Int. J. Energy Res.* **2022**, *46*, 13152.
[12] X. Wang, Z. Zhang, B. Xi, W. Chen, Y. Jia, J. Feng, S. Xiong, *ACS Nano* **2021**, *15*, 9244.
[13] L. E. Blanc, D. Kundu, L. F. Nazar, *Joule* **2020**, *4*, 771.
[14] N. Wang, X. Qiu, J. Xu, J. Huang, Y. Cao, Y. Wang, *ACS Mater. Lett.* **2021**, *4*, 190.
[15] L. Dong, X. Ma, Y. Li, L. Zhao, W. Liu, J. Cheng, C. Xu, B. Li, Q.-H. Yang, F. Kang, *Energy Storage Mater.* **2018**, *13*, 96.
[16] X. Ma, J. Cheng, L. Dong, W. Liu, J. Mou, L. Zhao, J. Wang, D. Ren, J. Wu, C. Xu, F. Kang, *Energy Storage Mater.* **2019**, *20*, 335.
[17] H. Tang, J. Yao, Y. Zhu, *Adv. Energy Mater.* **2021**, *11*, 2003994.
[18] J. Zheng, Z. Huang, F. Ming, Y. Zeng, B. Wei, Q. Jiang, Z. Qi, Z. Wang, H. Liang, *Small* **2022**, *18*, 2200006.
[19] Y. Zhao, L. Ma, Y. Zhu, P. Qin, H. Li, F. Mo, D. Wang, G. Liang, Q. Yang, W. Liu, C. Zhi, *ACS Nano* **2019**, *13*, 7270.
[20] X. Wang, M. Salari, D.-e. Jiang, J. Chapman Varela, B. Anasori, D. J. Wesolowski, S. Dai, M. W. Grinstaff, Y. Gogotsi, *Nat. Rev. Mater.* **2020**, *5*, 787.
[21] Z. Xing, Y. Sun, X. Xie, Y. Tang, G. Xu, J. Han, B. Lu, S. Liang, G. Chen, J. Zhou, *Angew. Chem., Int. Ed.* **2022**, *62*, e202215324.
[22] Q. Zhang, Y. Su, Z. Shi, X. Yang, J. Sun, *Small* **2022**, *18*, 2203583.
[23] L. Wang, X. Wang, B. Song, Z. Wang, L. Zhang, Q. Lu, *Surf. Interfaces* **2022**, *33*, 102222.
[24] J. Huang, H. Liang, Y. Tang, B. Lu, J. Zhou, S. Liang, *Adv. Energy Mater.* **2022**, *12*, 2201434.
[25] L. Hong, L. Y. Wang, Y. Wang, X. Wu, W. Huang, Y. Zhou, K. X. Wang, J. S. Chen, *Adv. Sci.* **2022**, *9*, 2104866.
[26] Z. Bie, Q. Yang, X. X. Cai, Z. Chen, Z. Y. Jiao, J. B. Zhu, Z. F. Li, J. Z. Liu, W. X. Song, C. Y. Zhi, *Adv. Energy Mater.* **2022**, *12*, 2202683.
[27] T. Liu, Z. Xu, L. Chen, Y. Zhang, M. Wang, Y. Jia, Y. Huang, *J. Colloid Interface Sci.* **2022**, *613*, 524.
[28] N. N. Zhang, S. Huang, Z. S. Yuan, J. C. Zhu, Z. F. Zhao, Z. Q. Niu, *Angew. Chem., Int. Ed.* **2021**, *60*, 2861.
[29] H. B. He, H. Y. Qin, J. Wu, X. F. Chen, R. S. Huang, F. Shen, Z. R. Wu, G. N. Chen, S. B. Yin, J. Liu, *Energy Storage Mater.* **2021**, *43*, 317.
[30] S. Guo, L. Qin, T. Zhang, M. Zhou, J. Zhou, G. Fang, S. Liang, *Energy Storage Mater.* **2021**, *34*, 545.
[31] Y. Du, Y. Li, B. B. Xu, T. X. Liu, X. Liu, F. Ma, X. Gu, C. Lai, *Small* **2022**, *18*, 2104640.
[32] R. Z. Qin, Y. T. Wang, L. Yao, L. Y. Yang, Q. H. Zhao, S. X. Ding, L. L. Liu, F. Pan, *Nano Energy* **2022**, *98*, 107333.
[33] M. Zhou, Y. Chen, G. Fang, S. Liang, *Energy Storage Mater.* **2022**, *45*, 618.
[34] Z. Zhao, J. Zhao, Z. Hu, J. Li, J. Li, Y. Zhang, C. Wang, G. Cui, *Energy Environ. Sci.* **2019**, *12*, 1938.
[35] Y. Song, P. Ruan, C. Mao, Y. Chang, L. Wang, L. Dai, P. Zhou, B. Lu, J. Zhou, Z. He, *Nano-Micro Lett.* **2022**, *14*, 218.
[36] Y. Zhang, Z. Huang, K. Wu, F. Yu, M. Zhu, G. Wang, G. Xu, M. Wu, H.-K. Liu, S.-X. Dou, C. Wu, *Chem. Eng. J.* **2022**, *430*, 133042.
[37] T. Liu, J. Hong, J. Wang, Y. Xu, Y. Wang, *Energy Storage Mater.* **2022**, *45*, 1074.
[38] P. Wang, X. Xie, Z. Xing, X. Chen, G. Fang, B. Lu, J. Zhou, S. Liang, H. J. Fan, *Adv. Energy Mater.* **2021**, *11*, 2101158.
[39] V. Soundharrajan, B. Sambandam, S. Kim, S. Islam, J. Jo, S. Kim, V. Mathew, Y.-k. Sun, J. Kim, *Energy Storage Mater.* **2020**, *28*, 407.
[40] M. Li, K. Xie, R. Peng, B. Yuan, Q. Wang, C. Wang, *Small* **2022**, *18*, 2107398.
[41] B. Anasori, M. R. Lukatskaya, Y. Gogotsi, *Nat. Rev. Mater.* **2017**, *2*, 16098.
[42] M. Naguib, M. Kurtoglu, V. Presser, J. Lu, J. Niu, M. Heon, L. Hultman, Y. Gogotsi, M. W. Barsoum, *Adv. Mater.* **2011**, *23*, 4248.
[43] X. L. Li, Z. D. Huang, C. E. Shuck, G. J. Liang, Y. Gogotsi, C. Y. Zhi, *Nat. Rev. Chem.* **2022**, *6*, 389.
[44] J. Pang, R. G. Mendes, A. Bachmatiuk, L. Zhao, H. Q. Ta, T. Gemming, H. Liu, Z. Liu, M. H. Rummeli, *Chem. Soc. Rev.* **2019**, *48*, 72.
[45] M. K. Aslam, Y. Niu, M. Xu, *Adv. Energy Mater.* **2020**, *11*, 2000681.
[46] X. Wang, L. Bannenberg, *MRS Bull.* **2021**, *46*, 755.
[47] R. Guo, X. Han, P. Yuan, X. He, Q. Li, J. Sun, L. Dang, Z. Liu, Y. Zhang, Z. Lei, *Nano Res.* **2021**, *15*, 3254.
[48] R. Guo, P. Yuan, X. Han, X. He, J. Lu, Q. Li, L. Dang, J. Sun, Z. Liu, Z. Lei, *Small* **2023**, *19*, 2205947.
[49] T. S. Mathis, K. Maleski, A. Goad, A. Sarycheva, M. Anayee, A. C. Foucher, K. Hantanasirisakul, C. E. Shuck, E. A. Stach, Y. Gogotsi, *ACS Nano* **2021**, *15*, 6420.
[50] F. Ming, H. Liang, G. Huang, Z. Bayhan, H. N. Alshareef, *Adv. Mater.* **2021**, *33*, 2004039.
[51] X. Zhu, X. Li, M. L. K. Essandoh, J. Tan, Z. Cao, X. Zhang, P. Dong, P. M. Ajayan, M. Ye, J. Shen, *Energy Storage Mater.* **2022**, *50*, 243.
[52] X. Li, M. Li, K. Luo, Y. Hou, P. Li, Q. Yang, Z. Huang, G. Liang, Z. Chen, S. Du, Q. Huang, C. Zhi, *ACS Nano* **2022**, *16*, 813.
[53] X. Li, M. Li, Q. Yang, D. Wang, L. Ma, G. Liang, Z. Huang, B. Dong, Q. Huang, C. Zhi, *Adv. Energy Mater.* **2020**, *10*, 2001394.
[54] M. Li, X. Li, G. Qin, K. Luo, J. Lu, Y. Li, G. Liang, Z. Huang, J. Zhou, L. Hultman, P. Eklund, P. O. Å. Persson, S. Du, Z. Chai, C. Zhi, Q. Huang, *ACS Nano* **2021**, *15*, 1077.
[55] W. Du, L. Miao, Z. Song, X. Zheng, Y. Lv, D. Zhu, L. Gan, M. Liu, *J. Power Sources* **2022**, *536*, 231512.
[56] Y. An, Y. Tian, C. Liu, S. Xiong, J. Feng, Y. Qian, *ACS Nano* **2021**, *15*, 15259.
[57] M. H. Zhang, W. Xu, L. S. Wu, Y. F. Dong, *New Carbon Mater.* **2022**, *37*, 508.
[58] J. Chen, Y. Ding, D. Yan, J. Huang, S. Peng, *SusMat* **2022**, *2*, 293.
[59] Y. Liu, S. Wang, Z. Huang, X. Yang, R. Zhang, X. Liu, S. Lu, X. Ma, *J. Mater. Sci.* **2022**, *57*, 13817.
[60] X. Li, X. Ma, Y. Hou, Z. Zhang, Y. Lu, Z. Huang, G. Liang, M. Li, Q. Yang, J. Ma, N. Li, B. Dong, Q. Huang, F. Chen, J. Fan, C. Zhi, *Joule* **2021**, *5*, 2993.
[61] M. Ye, J. Shen, X. Zhu, Z. Cao, W. Wang, H. Li, J. Dong, S. Gao, D. Xu, L. Li, *ACS Nano* **2021**, *15*, 2971.
[62] J. Zhou, M. Xie, F. Wu, Y. Mei, Y. Hao, L. Li, R. Chen, *Adv. Mater.* **2022**, *34*, 2106897.
[63] H. Chen, M. Chen, W. Zhou, X. Han, B. Liu, W. Zhang, J. Chen, *ACS Appl. Mater. Interfaces* **2022**, *14*, 6876.
[64] Y. W. Su, B. Z. Liu, Q. H. Zhang, J. Peng, C. H. Wei, S. Li, W. P. Li, Z. K. Xue, X. Z. Yang, J. Y. Sun, *Adv. Funct. Mater.* **2022**, *32*, 2204306.
[65] Y. Wang, Z. Wang, F. Yang, S. Liu, S. Zhang, J. Mao, Z. Guo, *Small* **2022**, *18*, 2107033.
[66] L. Zhou, F. Wang, F. Yang, X. Liu, Y. Yu, D. Zheng, X. Lu, *Angew. Chem., Int. Ed.* **2022**, *61*, e202208051.

[67] J. Hao, X. Li, X. Zeng, D. Li, J. Mao, Z. Guo, *Energy Environ. Sci.* **2020**, *13*, 3917.
[68] X. Jia, C. Liu, Z. G. Neale, J. Yang, G. Cao, *Chem. Rev.* **2020**, *120*, 7795.
[69] B. Tang, L. Shan, S. Liang, J. Zhou, *Energy Environ. Sci.* **2019**, *12*, 3288.
[70] J. Yang, B. Yin, Y. Sun, H. Pan, W. Sun, B. Jia, S. Zhang, T. Ma, *Nano-Micro Lett.* **2022**, *14*, 42.
[71] D. Selvakumaran, A. Pan, S. Liang, G. Cao, *J. Mater. Chem. A* **2019**, *7*, 18209.
[72] L. Chen, Q. An, L. Mai, *Adv. Mater. Interfaces* **2019**, *6*, 1900387.
[73] W. Shi, W. S. V. Lee, J. Xue, *ChemSusChem* **2021**, *14*, 1634.
[74] X. Chen, P. Ruan, X. Wu, S. Liang, J. Zhou, *Acta Phys.-Chim. Sin.* **2021**, *38*, 2111003.
[75] B. Lee, H. R. Lee, H. Kim, K. Y. Chung, B. W. Cho, S. H. Oh, *Chem. Commun.* **2015**, *51*, 9265.
[76] X. Gao, H. Wu, W. Li, Y. Tian, Y. Zhang, H. Wu, L. Yang, G. Zou, H. Hou, X. Ji, *Small* **2020**, *16*, 1905842.
[77] W. Sun, F. Wang, S. Hou, C. Yang, X. Fan, Z. Ma, T. Gao, F. Han, R. Hu, M. Zhu, C. Wang, *J. Am. Chem. Soc.* **2017**, *139*, 9775.
[78] D. Kundu, S. Hosseini Vajargah, L. Wan, B. Adams, D. Prendergast, L. F. Nazar, *Energy Environ. Sci.* **2018**, *11*, 881.
[79] S. Zhao, B. Han, D. Zhang, Q. Huang, L. Xiao, L. Chen, D. G. Ivey, Y. Deng, W. Wei, *J. Mater. Chem. A* **2018**, *6*, 5733.
[80] F. Wan, Z. Q. Niu, *Angew. Chem., Int. Ed.* **2019**, *58*, 16358.
[81] Y. Yang, Y. Tang, G. Fang, L. Shan, J. Guo, W. Zhang, C. Wang, L. Wang, J. Zhou, S. Liang, *Energy Environ. Sci.* **2018**, *11*, 3157.
[82] Z. Li, S. Ganapathy, Y. Xu, Z. Zhou, M. Sarilar, M. Wagemaker, *Adv. Energy Mater.* **2019**, *9*, 1900237.
[83] G. Li, Z. Yang, Y. Jiang, C. Jin, W. Huang, X. Ding, Y. Huang, *Nano Energy* **2016**, *25*, 211.
[84] L. Ou, H. Ou, M. Qin, Z. Liu, G. Fang, X. Cao, S. Liang, *ChemSusChem* **2022**, *15*, 202201184.
[85] J. Yin, W. Zhang, N. A. Alhebshi, N. Salah, H. N. Alshareef, *Adv. Energy Mater.* **2021**, *11*, 2100201.
[86] Y. Tian, R. Amal, D.-W. Wang, *Front. Energy Res.* **2016**, *4*, 34.
[87] X. Chen, H. Zhang, Y. Gao, J. H. Liu, X. Cao, C. Zhan, S. Wang, J. Wang, S. X. Dou, D. Cao, *Carbon Neutralization* **2022**, *1*, 159.
[88] J. Yan, E. H. Ang, Y. Yang, Y. Zhang, M. Ye, W. Du, C. C. Li, *Adv. Funct. Mater.* **2021**, *31*, 2010213.
[89] D. Chen, M. Lu, D. Cai, H. Yang, W. Han, *J. Energy Chem.* **2021**, *54*, 712.
[90] G. Fang, J. Zhou, A. Pan, S. Liang, *ACS Energy Lett.* **2018**, *3*, 2480.
[91] J. Cao, D. Zhang, X. Zhang, Z. Zeng, J. Qin, Y. Huang, *Energy Environ. Sci.* **2022**, *15*, 499.
[92] N. Guo, W. Huo, X. Dong, Z. Sun, Y. Lu, X. Wu, L. Dai, L. Wang, H. Lin, H. Liu, H. Liang, Z. He, Q. Zhang, *Small Methods* **2022**, *6*, 2200597.
[93] Y. Zuo, K. Wang, P. Pei, M. Wei, X. Liu, Y. Xiao, P. Zhang, *Mater. Today Energy* **2021**, *20*, 100692.
[94] Q. Yang, Q. Li, Z. Liu, D. Wang, Y. Guo, X. Li, Y. Tang, H. Li, B. Dong, C. Zhi, *Adv. Mater.* **2020**, *32*, 2001854.
[95] Z. Yang, C. Lv, W. Li, T. Wu, Q. Zhang, Y. Tang, M. Shao, H. Wang, *Small* **2022**, *18*, 2104148.
[96] H. Ge, X. Feng, D. Liu, Y. Zhang, *Nano Res. Energy* **2023**, *2*, e9120039.
[97] W. Lu, C. Xie, H. Zhang, X. Li, *ChemSusChem* **2018**, *11*, 3996.
[98] Z. Du, C. Wu, Y. Chen, Z. Cao, R. Hu, Y. Zhang, J. Gu, Y. Cui, H. Chen, Y. Shi, J. Shang, B. Li, S. Yang, *Adv. Mater.* **2021**, *33*, 2101473.
[99] C. Deng, X. Xie, J. Han, B. Lu, S. Liang, J. Zhou, *Adv. Funct. Mater.* **2021**, *31*, 2103227.
[100] A. Bayaguud, Y. Fu, C. Zhu, *J. Energy Chem.* **2022**, *64*, 246.
[101] M. Zhou, C. Fu, L. Qin, Q. Ran, S. Guo, G. Fang, X. Lang, Q. Jiang, S. Liang, *Energy Storage Mater.* **2022**, *52*, 161.
[102] D. L. Chao, W. H. Zhou, C. Ye, Q. H. Zhang, Y. G. Chen, L. Gu, K. Davey, S. Z. Qiao, *Angew. Chem., Int. Ed.* **2019**, *58*, 7823.
[103] Y. Yu, W. Xu, X. Liu, X. Lu, *Adv. Sustainable Syst.* **2020**, *4*, 2000082.
[104] N. Zhang, X. Chen, M. Yu, Z. Niu, F. Cheng, J. Chen, *Chem. Soc. Rev.* **2020**, *49*, 4203.
[105] W. Du, E. H. Ang, Y. Yang, Y. Zhang, M. Ye, C. C. Li, *Energy Environ. Sci.* **2020**, *13*, 3330.
[106] L. Ma, Q. Li, Y. Ying, F. Ma, S. Chen, Y. Li, H. Huang, C. Zhi, *Adv. Mater.* **2021**, *33*, 2007406.
[107] B.-F. Cui, X.-P. Han, W.-B. Hu, *Small Struct.* **2021**, *2*, 2000128.
[108] W. Lu, C. Zhang, H. Zhang, X. Li, *ACS Energy Lett.* **2021**, *6*, 2765.
[109] J. Zhou, M. Xie, F. Wu, Y. Mei, Y. Hao, R. Huang, G. Wei, A. Liu, L. Li, R. Chen, *Adv. Mater.* **2021**, *33*, 2101649.
[110] P. Chen, X. Yuan, Y. Xia, Y. Zhang, L. Fu, L. Liu, N. Yu, Q. Huang, B. Wang, X. Hu, Y. Wu, T. van Ree, *Adv. Sci.* **2021**, *8*, 2100309.
[111] M. Okubo, A. Sugahara, S. Kajiyama, A. Yamada, *Acc. Chem. Res.* **2018**, *51*, 591.
[112] Q. Yang, Z. Huang, X. Li, Z. Liu, H. Li, G. Liang, D. Wang, Q. Huang, S. Zhang, S. Chen, C. Zhi, *ACS Nano* **2019**, *13*, 8275.
[113] P. A. Maughan, N. Tapia-Ruiz, N. Bimbo, *Electrochim. Acta* **2020**, *341*, 136061.
[114] X. Li, M. Li, Q. Yang, H. Li, H. Xu, Z. Chai, K. Chen, Z. Liu, Z. Tang, L. Ma, Z. Huang, B. Dong, X. Yin, Q. Huang, C. Zhi, *ACS Nano* **2020**, *14*, 541.
[115] B. Gavriel, N. Shpigel, F. Malchik, G. Bergman, M. Turgeman, M. D. Levi, D. Aurbach, *Energy Storage Mater.* **2021**, *38*, 535.
[116] Q. Shan, X. Mu, M. Alhabeb, C. E. Shuck, D. Pang, X. Zhao, X.-F. Chu, Y. Wei, F. Du, G. Chen, Y. Gogotsi, Y. Gao, Y. Dall'Agnese, *Electrochem. Commun.* **2018**, *96*, 103.
[117] X. Li, M. Li, Q. Yang, G. Liang, Z. Huang, L. Ma, D. Wang, F. Mo, B. Dong, Q. Huang, C. Zhi, *Adv. Energy Mater.* **2020**, *10*, 2001791.
[118] A. S. Etman, J. Halim, J. Rosen, *Mater. Today Energy* **2021**, *22*, 100878.
[119] S. K. Nemani, B. W. Zhang, B. C. Wyatt, Z. D. Hood, S. Manna, R. Khaledialidusti, W. C. Hong, M. G. Sternberg, S. Sankaranarayanan, B. Anasori, *ACS Nano* **2021**, *15*, 12815.
[120] A. S. Etman, J. Zhou, J. Rosen, *Electrochem. Commun.* **2022**, *137*, 107264.
[121] X. Hui, X. Ge, R. Zhao, Z. Li, L. Yin, *Adv. Funct. Mater.* **2020**, *30*, 2005190.
[122] W. Liu, L. Li, C. Hu, D. Chen, G. Shen, *Adv. Mater. Technol.* **2022**, *7*, 2200158.
[123] S. Li, Q. Shi, Y. Li, J. Yang, T. H. Chang, J. Jiang, P. Y. Chen, *Adv. Funct. Mater.* **2020**, *30*, 2003721.
[124] M. Peng, L. Wang, L. Li, X. Tang, B. Huang, T. Hu, K. Yuan, Y. Chen, *Adv. Funct. Mater.* **2022**, *32*, 2109524.
[125] Y. B. Li, H. Shao, Z. F. Lin, J. Lu, L. Y. Liu, B. Duployer, P. O. A. Persson, P. Eklund, L. Hultman, M. Li, K. Chen, X. H. Zha, S. Y. Du, P. Rozier, Z. F. Chai, E. Raymundo-Pinero, P. L. Taberna, P. Simon, Q. Huang, *Nat. Mater.* **2021**, *20*, 571.
[126] M. Li, J. Lu, K. Luo, Y. Li, K. Chang, K. Chen, J. Zhou, J. Rosen, L. Hultman, P. Eklund, P. O. A. Persson, S. Du, Z. Chai, Z. Huang, Q. Huang, *J. Am. Chem. Soc.* **2019**, *141*, 4730.
[127] V. Kamysbayev, A. S. Filatov, H. C. Hu, X. Rui, F. Lagunas, D. Wang, R. F. Klie, D. V. Talapin, *Science* **2020**, *369*, 979.
[128] X. Li, M. Li, Z. Huang, G. Liang, Z. Chen, Q. Yang, Q. Huang, C. Zhi, *Energy Environ. Sci.* **2021**, *14*, 407.
[129] X. Li, N. Li, Z. Huang, Z. Chen, Y. Zhao, G. Liang, Q. Yang, M. Li, Q. Huang, B. Dong, J. Fan, C. Zhi, *ACS Nano* **2021**, *15*, 1718.
[130] X. Li, N. Li, Z. Huang, Z. Chen, G. Liang, Q. Yang, M. Li, Y. Zhao, L. Ma, B. Dong, Q. Huang, J. Fan, C. Zhi, *Adv. Mater.* **2021**, *33*, 2006897.
[131] W. Kou, L. Yu, Q. Wang, Y. Yang, T. Yang, H. Geng, X. Miao, B. Gao, G. Yang, *J. Power Sources* **2022**, *520*, 230872.
[132] Y. Feng, Y. Feng, Y. Zhang, L. Sun, X. Li, M. Meng, Y. Zhu, K. Liu, *J. Power Sources* **2022**, *545*, 231944.
[133] P. Liang, T. Xu, K. Zhu, Y. Rao, H. Zheng, M. Wu, J. Chen, J. Liu, K. Yan, J. Wang, R. Zhang, *Energy Storage Mater.* **2022**, *50*, 63.

[134] H. Liu, L. Jiang, B. Cao, H. Du, H. Lu, Y. Ma, H. Wang, H. Guo, Q. Huang, B. Xu, S. Guo, *ACS Nano* **2022**, *16*, 14539.
[135] Z. Shi, Q. Ru, Z. Pan, M. Zheng, F. Chi-Chun Ling, L. Wei, *ChemElectroChem* **2021**, *8*, 1091.
[136] J. Chen, B. Xiao, C. Hu, H. Chen, J. Huang, D. Yan, S. Peng, *ACS Appl. Mater. Interfaces* **2022**, *14*, 28760.
[137] X. Zhu, W. Wang, Z. Cao, S. Gao, M. O. L. Chee, X. Zhang, P. Dong, P. M. Ajayan, M. Ye, J. Shen, *J. Mater. Chem. A* **2021**, *9*, 17994.
[138] D. Sha, C. Lu, W. He, J. Ding, H. Zhang, Z. Bao, X. Cao, J. Fan, Y. Dou, L. Pan, Z. Sun, *ACS Nano* **2022**, *16*, 2711.
[139] S. L. Wang, Q. Wang, W. Zeng, M. Wang, L. M. Ruan, Y. A. Ma, *Nano-Micro Lett.* **2019**, *11*, 70.
[140] C. Sun, C. P. Wu, X. X. Gu, C. Wang, Q. H. Wang, *Nano-Micro Lett.* **2021**, *13*, 89.
[141] X. Li, Q. Li, Y. Hou, Q. Yang, Z. Chen, Z. Huang, G. Liang, Y. Zhao, L. Ma, M. Li, Q. Huang, C. Zhi, *ACS Nano* **2021**, *15*, 14631.
[142] Y. Tian, Y. An, Y. Yang, B. Xu, *Energy Storage Mater.* **2022**, *49*, 122.
[143] Y. Zhang, Z. Cao, S. Liu, Z. Du, Y. Cui, J. Gu, Y. Shi, B. Li, S. Yang, *Adv. Energy Mater.* **2022**, *12*, 2103979.
[144] L. Tan, C. Wei, Y. Zhang, Y. An, S. Xiong, J. Feng, *Chem. Eng. J.* **2022**, *431*, 134277.
[145] N. Wang, Z. Wu, Y. Long, D. Chen, C. Geng, X. Liu, D. Han, J. Zhang, Y. Tao, Q.-H. Yang, *J. Energy Chem.* **2022**, *73*, 277.
[146] K. Li, M. Liang, H. Wang, X. Wang, Y. Huang, J. Coelho, S. Pinilla, Y. Zhang, F. Qi, V. Nicolosi, Y. Xu, *Adv. Funct. Mater.* **2020**, *30*, 2000842.
[147] J.-L. Yang, P. Yang, W. Yan, J.-W. Zhao, H. J. Fan, *Energy Storage Mater.* **2022**, *51*, 259.
[148] J. M. Park, M. Jana, S. H. Baek, T. Kang, P. Xiong, J. H. Park, J. S. Kim, A. S. Zeraati, M. Shekhirev, P. V. Braun, Y. Gogotsi, H. S. Park, *J. Energy Chem.* **2023**, *76*, 187.
[149] Z. Li, D. Guo, D. Wang, M. Sun, H. Sun, *J. Power Sources* **2021**, *506*, 230197.
[150] W. Li, K. Wang, S. Cheng, K. Jiang, *Adv. Energy Mater.* **2019**, *9*, 1900993.
[151] Y. Tian, Y. An, C. Wei, B. Xi, S. Xiong, J. Feng, Y. Qian, *Adv. Energy Mater.* **2020**, *11*, 2002529.
[152] X. Wang, Y. Wang, Y. Jiang, X. Li, Y. Liu, H. Xiao, Y. Ma, Y. y. Huang, G. Yuan, *Adv. Funct. Mater.* **2021**, *31*, 2103210.
[153] B. Zhao, S. Wang, Q. Yu, Q. Wang, M. Wang, T. Ni, L. Ruan, W. Zeng, *J. Power Sources* **2021**, *504*, 230076.
[154] Y. Tian, Y. An, C. Liu, S. Xiong, J. Feng, Y. Qian, *Energy Storage Mater.* **2021**, *41*, 343.
[155] Y. Tian, Y. An, C. Wei, B. Xi, S. Xiong, J. Feng, Y. Qian, *ACS Nano* **2019**, *13*, 11676.
[156] Y. L. An, Y. Tian, Q. Y. Man, H. T. Shen, C. K. Liu, Y. Qian, S. L. Xiong, J. K. Feng, Y. T. Qian, *ACS Nano* **2022**, *16*, 6755.
[157] F. Ming, Y. Zhu, G. Huang, A. H. Emwas, H. Liang, Y. Cui, H. N. Alshareef, *J. Am. Chem. Soc.* **2022**, *144*, 7160.
[158] G. Wang, M. Zhu, G. Chen, Z. Qu, B. Kohn, U. Scheler, X. Chu, Y. Fu, O. G. Schmidt, X. Feng, *Adv. Mater.* **2022**, *34*, 2201957.
[159] H. Chen, W. Zhou, M. Chen, Q. Tian, X. Han, J. Chen, *Nano Res.* **2022**, *16*, 536.

Rui Guo received her bachelor's degree in complex materials and engineering from Tiangong University in 2016. She passed the master-doctor program in 2018, and now she is a Ph.D. student supervised by professor Zhibin Lei at Materials Physics and Chemistry, Shaanxi Normal University. Supported by the China Scholarship Council, she was a Joint-Supervision Ph.D. student supervised by Dr. Xuehang Wang at Applied Sciences, Delft University of Technology in the year of 2021–2022. Her research topic mainly focuses on the design and synthesis of nanostructured carbon/MXene-based electrodes for flexible supercapacitors and aqueous zinc ion storage.

Chaofan Chen is a Ph.D. student supervised by Dr. Xuehang Wang in the Department of Radiation Science and Technology at Delft University of Technology. She received her master's degree in condensed matter physics from Jilin University in 2021. Her research interest mainly focuses on understanding the interfacial structure and electrochemical performance of 2D MXene-based materials.

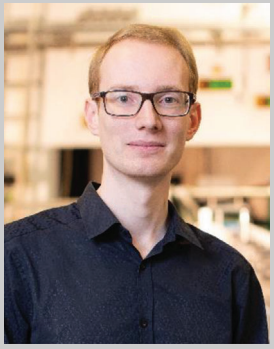

Lars Bannenberg is an assistant professor at Delft University of Technology, The Netherlands. Lars received his M.Sc. in financial economics from Erasmus University Rotterdam in 2015, as well as M.Sc. (2015) and Ph.D. degrees (2019) in applied physics from Delft University of Technology. His research interests include thin film materials and interfaces of energy materials such as batteries and materials for optical hydrogen sensors. To study these materials, Lars uses a wide range of neutron- and X-ray scattering techniques. At present, he is also responsible for the neutron reflectometer at the Reactor Institute Delft.

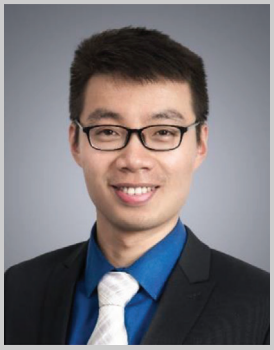

Minghao Yu received his Ph.D. degree in material physics and chemistry from Sun Yat-sen University in June 2017. In March 2019, he became a research group leader of the Chair for Molecular Functional Materials at Technische Universität Dresden. His research interests focus on the development of advanced functional materials for applications of energy storage (supercapacitors and metal-ion batteries) and conversion (electrocatalysis and metal-air batteries).

Zdenek Sofer is a tenured professor at the University of Chemistry and Technology Prague since 2019. He received his Ph.D. in 2008 and during his Ph.D. he spent one year at the Forschungszentrum Jülich and also one postdoctoral stay at University Duisburg-Essen, Germany. Research interests of Prof. Sofer are concerning 2D materials including graphene, layered chalcogenides and other 2D materials, its crystal growth and chemical modifications. His research covers various applications of 2D materials including energy storage and conversion. He is an associated editor of FlatChem journal. He has published over 570 articles, which received over 23 000 citations (h-index 77).

Zhibin Lei received his Ph.D. of physical chemistry at the University of Science and Technology of China in 2002. Then he worked as a postdoctoral fellow at Dalian Institute of Chemical Physics, Chinese Academy of Sciences (2002-2004). He was promoted to a full professor in 2007, and then worked as a senior research fellow at the Department of Chemical & Biomolecular Engineering, National University of Singapore (2009-2011). He is currently a full professor at the School of Materials Science and Engineering, Shaanxi Normal University. His current research interests focus on the design of flexible electrodes and devices for electrochemical energy storage.

Xuehang Wang is an assistant professor in the Department of Radiation Science and Technology at Delft University of Technology. She earned her Ph.D. in chemical engineering from the Norwegian University of Science and Technology in 2016 and was a postdoctoral researcher at A.J. Drexel Nanomaterials Institute, Drexel University from 2017 to 2020. Her research focuses on gaining an understanding of the charge mechanisms of energy storage devices, particularly the electrolyte transport at the electrode-electrolyte interfaces of 2D MXenes and various carbon materials.